Water Research 287 (2025) 124320

Contents lists available at ScienceDirect

Water Research

journal homepage: www.elsevier.com/locate/watres

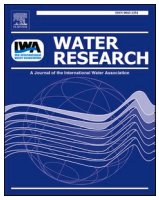

Elevated in-stream CO_2 concentration stimulates net-N_2O production from global fluvial ecosystems

R.M. Mwanake [a], G.M. Gettel [b,d], E.G. Wangari [a], G.W. Macharia [e], R. Martínez-Cuesta [f,g], S. Schulz [f], M. Schloter [f,g], K. Butterbach-Bahl [a,c], R. Kiese [a,*]

[a] Karlsruhe Institute of Technology, Institute for Meteorology and Climate Research, Atmospheric Environmental Research (IMK-IFU); Garmisch-Partenkirchen, Germany
[b] IHE Delft Institute for Water Education, Department of Water Resources and Ecosystems, Delft, the Netherlands
[c] Pioneer Center Land-CRAFT, Department of Agroecology, University of Aarhus, Aarhus, Denmark
[d] Aarhus University, Department of Ecoscience, Aquatic Ecology Section, Aarhus, Denmark
[e] The Kenyan Institute: National Water Harvesting & Storage Authority; Nairobi, Kenya
[f] Helmholtz Zentrum München Deutsches Forschungszentrum für Gesundheit und Umwelt, Research Unit Comparative Microbiome Analysis; Neuherberg, Germany
[g] Chair of Environmental Microbiology, TUM School of Life Science, Technical University of Munich; Freising, Germany

ARTICLE INFO

Keywords:
Nitrification
Denitrification
Climate feedback
Anthropogenic influence
Carbon and nitrogen cycling
Rivers
Greenhouse gases

ABSTRACT

Riverine CO_2 and N_2O concentrations have risen since pre-industrial times, yet their biogeochemical interactions remain unclear. This study found a positive correlation between N_2O and CO_2 saturation in fluvial ecosystems, which was absent at high DOC:NO_3 ratios. Low DOC:NO_3 ratios and high CO_2 saturation promote chemoautotrophic nitrification, suggesting its key role in riverine net N_2O production. In vitro experiments confirmed that elevated CO_2 enhances nitrification rates, nitrifier gene abundance, and N_2O fluxes, indicating that the CO_2 fertilization effect on N_2O production is a potential climate feedback. Under this effect, current global N_2O emissions may be underestimated by 12 % (interquartile range: 8 – 15) due to unaccounted nocturnal CO_2 increases. As land use change projections suggest the conversion of natural lands into croplands and urban areas, this CO_2-driven rise in riverine N_2O emissions could increase, amplifying the global impacts of land use on riverine greenhouse gas emissions.

1. Introduction

Since pre-industrial times, carbon dioxide (CO_2) and nitrous oxide (N_2O) concentrations in riverine ecosystems have risen, increasing the contributions of these ecosystems to global greenhouse gas (GHG) emissions (Regnier et al., 2013; Yao et al., 2020). The concurrent increase in the concentrations of these two gases can be associated with the fact that they may have similar responses to land use and hydrological controls (e.g., Mwanake et al., 2023a; Piatka et al., 2024). Land use changes from natural forests and wetlands to agricultural lands and human settlements boost the inflow of labile carbon and nutrients to rivers, favoring in-stream CO_2 and N_2O production (e.g., Drake et al., 2019; Regnier et al., 2013; Yao et al., 2020). At the same time, oversaturated soil water, groundwater, and wastewater sources of these gases can also be directly transported to rivers during periods of hydrological connectivity (Mwanake et al., 2022, 2023b; H. Zhang et al., 2022). However, the possibility that the positive co-variation in CO_2 and N_2O concentration in rivers could be related to a direct causal relationship between CO_2 availability and chemo-autotropic nitrification has not been investigated.

N_2O production via nitrification in rivers can occur during ammonium oxidation. In this step, ammonium (NH_4-N) is oxidized by ammonium oxidizing bacteria (AOB) or archaea (AOA) to hydroxylamine (NH_2OH) and subsequently to nitrite (NO_2-N). The oxidation of NH_2OH or the reduction of the NO_2-N results in the formation of N_2O (Quick et al., 2019). The rate of N_2O production from ammonium oxidation depends on the abundance of ammonium oxidizers. The activity and growth of ammonium oxidizers require ammonium, oxic conditions, and the fixation of CO_2 mainly via the Calvin-Benson-Bassham (CBB) cycle for AOB and the 3-hydroxypropionate–4-hydroxybutyrate (HPHB) cycle for AOA. Compared to the HPHB cycle, the CBB cycle is more energy intensive, requiring 33 % more energy to fix one mole of CO_2. The higher energy demand of the CBB cycle is due to the inefficiency of the ribulose 1, 5-bisphosphate

* Corresponding author.
E-mail address: ralf.kiese@kit.edu (R. Kiese).

https://doi.org/10.1016/j.watres.2025.124320
Received 25 May 2025; Received in revised form 26 June 2025; Accepted 28 July 2025
Available online 29 July 2025

carboxylase/oxygenase (RubisCO) enzyme in catalyzing the reaction and the low affinity of the enzyme for CO_2. Therefore, ample supplies of CO_2 are required to overcome these limitations (Robert Tabita, 1999). Furthermore, RubisCO can only use aqueous CO_2 as a substrate, not HCO_3^- (Cooper et al., 1969), requiring an additional energy-consuming step in which HCO_3^- is actively transported to the cytoplasm and catalytically converted to aqueous CO_2 by the enzyme carbonic anhydrase. As HCO_3^- is the most abundant form of inorganic carbon in fluvial ecosystems characterized by circumneutral (pH:~7) waters (Raymond and Hamilton, 2018), the low availability of aqueous CO_2 in these ecosystems may limit the growth of ammonium oxidizers, particularly AOB, as has been shown in wastewater treatment systems (Steuernagel et al., 2018).

Apart from NH_2OH oxidation, which is either part of the nitrification process or may occur chemically (e.g., Wei et al., 2022), N_2O may be produced by AOB via a process called nitrifier denitrification, as AOB harbors the genes and enzymes homologous to those found in denitrifiers (Casciotti and Ward, 2001, 2005). This additional mechanism for N_2O production in AOB suggests that their N_2O yields may be greater than AOA's. Elevated in-stream CO_2 concentrations may directly increase N_2O production from AOB through nitrifier denitrification as it facilitates passive CO_2 fixation via the CBB cycle, thereby freeing up excess electrons for the process. Evidence for the stimulation of nitrification and N_2O production by elevated CO_2 has been reported in laboratory experiments focused on wastewater treatment (Denecke and Liebig, 2003; Jiang et al., 2015; Steuernagel et al., 2018) but has not yet been shown in riverine ecosystems. For example, Denecke and Liebig (2003) found optimum AOB growth rates in a mixed autotrophic-heterotrophic sludge reactor when CO_2 concentrations in the medium ranged from 0.01–1.04 mmol CO_2 L^{-1}, significantly enhancing rates of nitrite/nitrate formation. At the same time, higher N_2O yields from nitrification through the growth enhancement of a pure AOB culture were found in a laboratory chemostat experiment when gaseous CO_2 was the supplied carbon source instead of HCO_3^- (Jiang et al., 2015). Because N_2O yields from denitrification also depend on in-stream nitrate concentrations, increased nitrate turnover through nitrification may also result in higher N_2O yields from denitrification (Cébron et al., 2005; Quick et al., 2019).

Although the theoretical evidence above suggests that N_2O production from nitrification-induced processes (ammonium oxidation, nitrifier denitrification, and coupled nitrification-incomplete denitrification) can be stimulated by increased CO_2 concentration in fluvial ecosystems, this effect may only become evident when environmental conditions favor nitrification, resulting in both NO_3 and N_2O accretion (e.g., Baulch et al., 2011; Mwanake et al., 2019). Previous fluvial research shows that the stoichiometric ratio between DOC and NO_3 may be used to identify favorable conditions for autotrophic nitrification and heterotrophic processes such as respiration and denitrification (Strauss et al., 2002; Strauss and Lamberti, 2002; Taylor and Townsend, 2010). At low DOC:NO_3 ratios of <2, heterotrophic microbes, including denitrifiers, are C-limited (Taylor and Townsend, 2010). Under these conditions, nitrifiers are better competitors for available ammonium as compared to the heterotrophic bacteria (Strauss et al., 2002; Strauss and Lamberti, 2002), leading to an accumulation of excess NO_3 due to nitrification and decreased heterotrophic NO_3 demand (Taylor and Townsend, 2010). At DOC:NO_3 ratios between 2 – 5, nitrification can still occur; however, denitrification may dominate NO_3 consumption derived from nitrification and external sources (Taylor and Townsend, 2010). These stoichiometric conditions are therefore conducive to denitrification, often resulting in net N_2O production (e.g., Chen et al., 2025; C. Wang et al., 2024). For example, Chen et al. (2025) found that in urban river segments, denitrification was responsible for the majority of N_2O emissions (60–76 %), while nitrification contributed less than 40 %. This dominance was attributed to higher NO_3 concentrations and increased abundance of N_2O-producing denitrification genes due to urbanization. A similar study in urban river-lake networks in China also revealed that denitrification was the primary source of N_2O emissions in urban rivers, whereas nitrification dominated N_2O hotspots in lakes and agricultural rivers (C. Wang et al., 2024). In contrast, at higher DOC:NO_3 >5, the general heterotrophic microbial population becomes more N-limited than C-limited, resulting in rapid NO_3 assimilation by the heterotrophic microbes (Taylor and Townsend, 2010). This conceptual understanding was expanded by including thermodynamic constraints related to reducing redox conditions, whereby at high DOC:NO_3 ratios, the growth of nitrifiers is O_2-limited as O_2 availability declines with increasing heterotrophic microbial activity (Helton et al., 2015), favoring NO_3 and N_2O consumption as terminal electron acceptors.

Despite the potential significance of riverine net N_2O production driven by chemoautotrophic nitrification, either as a precursor to higher NO_3 concentrations or as a direct contributor to N_2O (e.g., Hama-Aziz et al., 2017; Harrison and Matson, 2003; Mwanake et al., 2019, 2024; S. Wang et al., 2024; Winnick, 2021), its relative contribution and underlying environmental controls have received less attention than heterotrophic denitrification. This is because N_2O production rates from incomplete denitrification are assumed to be much higher than from nitrification (Quick et al., 2019). Such an assumption may not always be true, considering that ammonium-derived sources rather than nitrate-derived sources were recently shown to account for up to 69 % of N_2O production from global agricultural streams (S. Wang et al., 2024). Moreover, nitrification is a net N_2O-producing process, while heterotrophic denitrification may also result in N_2O consumption through its reduction to N_2 (e.g., Aho et al., 2023; Mwanake et al., 2019; S. Wang et al., 2024).

The overall objective of this study was to determine the effect of elevated in-stream CO_2 concentrations on net-N_2O production from global fluvial ecosystems and if such a relationship is linked to enhanced nitrification rates under favorable environmental conditions for the chemoautotrophic process. We hypothesized that elevated in-stream CO_2 would favor nitrification-induced net N_2O production when the environmental DOC:NO_3 ratios are low, particularly in streams of catchments dominated by human influences due to external nitrogen inputs. However, at high DOC:NO_3 ratios, the positive CO_2 effect would be absent, as reducing redox conditions and stoichiometric disadvantages will limit nitrification and favor N_2O consumption processes.

To test these hypotheses, we employed two approaches. First, we conducted a meta-analysis on a global dataset to examine the role of catchment land use in controlling the general spatial-temporal trends of fluvial N_2O and CO_2 concentrations, and asses the hypothesized positive relationship between the two GHGs along DOC:NO_3 ratio gradients that regulate nitrification rates. The global dataset comprised 4,158 data points (from 549 sites) across 24 published studies, based on field observations of N_2O and CO_2 concentrations from five continents (Fig. S7; Mwanake et al., 2019, 2022, 2023a; Stanley et al., 2023). Second, we employed experimental approaches to elucidate the mechanisms that may explain the stimulatory effect of CO_2 oversaturation on nitrification and net N_2O production rates in streams, where background water DOC:NO_3 ratios varied from low to high due to differences in land use. Specifically, we measured in vitro potential gross nitrification rates, N_2O concentrations, net N_2O production rates, and the gene abundances of ammonium oxidizers and denitrifiers under different dissolved CO_2 treatments representing concentrations within the global range.

2. Materials and methods

2.1. Meta-data analysis

2.1.1. Data compilation

For the metanalysis, we compiled 4158 data points (549 sites) from 24 published studies based on field observations of N_2O and CO_2 concentrations over five continents (Fig. S7). The studies must have also included simultaneous water chemistry measurements, such as NH_4-N, NO_3-N, and DOC, to be added to the final data set. We obtained many

data points (n = 2920) from an existing GHG concentration published data set (Stanley et al., 2023). Additional already published data (n = 1238), composed mainly of headwater stream sites, were included from the Mara River in Kenya and five catchments in Germany (Mwanake et al., 2019, 2022, 2023a).

2.1.2. Relationship of upstream land use/land cover on in-stream CO_2, N_2O and DOC:NO_3 ratios in the global data

To determine how land use/land cover affects the spatio-temporal heterogeneities of global riverine CO_2 saturation, N_2O saturation, and the DOC:NO_3 ratios, we carried out a simple analysis based on the global land use map for 2019 from the HILDA+ database (Winkler et al., 2021; https://doi.org/10.1594/PANGAEA.921846). First, we obtained catchment boundaries for all the sites in our global data from the global hydrobasin dataset (Level 12; retrieved October 7, 2024: https://www.hydrosheds.org/products/hydrobasins). Second, land use percentages for each site were calculated from the HILDA+ land use map, which contains six distinct land use classes: urban, cropland, forests, pasture, unmanaged grasslands, and sparse/no vegetation. The dominant land class for each catchment (>55 % of a single land use class) was then determined. Catchments that did not predominantly belong to one land use class were classified as mixed land use catchments. Comparisons of the three parameters across land use classes were based on pairwise mean comparisons using the non-parametric Wilcoxon test. All these analyses were performed in R version 4.3.2.

2.1.3. Statistical analyses linking CO_2 saturation to elevated N_2O production from nitrification

We used a linear mixed-effect model (LME) to determine the effects of CO_2 concentrations and DOC:NO_3 molar ratios, and their interactions (CO_2 * DOC:NO_3 ratios) on N_2O concentrations in the global dataset ("lme4" package in R version 4.3.2). In the model, the CO_2 * DOC:NO_3 interaction term was particularly interesting as it allowed us to test the significance of CO_2 oversaturation in increasing riverine N_2O concentrations while considering multiple DOC:NO_3 ratios where nitrification is either favored or inhibited. The CO_2 and N_2O concentrations used throughout our analyses were expressed as % saturation to correct for water temperature differences across the latitudinal gradient in the global data (Eq. (1). This calculation was done by normalizing their actual concentrations in the water (C_{aq} in moles L^{-1}) with the stream water concentrations in equilibrium with fixed atmospheric concentrations (421 ppm for CO_2 and 0.333 ppm for N_2O) and pressure (1atm) (C_{sat} in moles L^{-1}), based on Henry's gas solubility constants calculated at specific water temperatures.

$$GHG\ saturation\ (\%) = \left(\frac{C_{aq}}{C_{sat}}\right) \times 100 \quad (1)$$

Using fixed atmospheric concentrations may result in negligible to significant uncertainties in air-water GHG dynamics due to temporal or site-to-site differences in air temperature and barometric pressures (Reichenpfader and Attermeyer, 2024). However, this uncertainty was assumed to be minimal relative to water temperature changes, which we accounted for in the saturation calculations. In addition, we also tested the above relationships with molar concentrations, yielding similar conclusions, albeit with slightly different magnitudes in the effect sizes. Data for the overall statistical analyses were used as individual measurements for every site visit and not as catchment means. To ensure the validity of the effects of CO_2 and the DOC:NO_3 ratio on N_2O, the linear mixed-effects model structure included random effects of sampling dates and sites, thereby considering the vast geographical differences in the data (Fig. S7) and their temporal coverage (2001-07-02 to 2022-04-20). Model performances were assessed based on the normality of the residuals and the conditional r^2 (encompasses the variance explained by both fixed and random effects). Forest plots were then used to visualize the standardized effect sizes of the significant (p-value<0.05) fixed effects ("sjPlot" and "ggplot2" packages in R version 4.3.2). To visualize the CO_2 * DOC:NO_3 interaction effects in the global data predicted from the linear mixed effect model, multiple (n=20) N_2O-CO_2 slope ± SE values were generated ("interactions" package in R version 4.3.2), and their bivariate relationships with changing DOC:NO_3 ratios analyzed. Before model construction and evaluation, N_2O, CO_2, DOC:NO_3 ratios were always transformed using the natural logarithm to meet the normality assumption.

Multivariate path analysis from a structural equation model (SEM) was also used to unravel biogeochemical interactions amongst drivers of N_2O concentrations ("lavaan" package in R) (Mwanake et al., 2023a). In the SEM, the theoretical model consisted of several multivariate regression equations (Eqs. (2)–(7) based on relationships inferred in previous studies (Quick et al., 2019). Endogenous variables in the models, which directly influence in-stream biogeochemical N_2O production and consumption processes, included water physico-chemical variables such as DO % saturation that determines the redox conditions for biogeochemical reactions and NH_4-N, and NO_3-N concentrations that represent substrates for both nitrification and denitrification. The exogenous variables in the models, which affect in-stream N_2O concentrations directly as carbon sources for autotrophic and heterotrophic production or indirectly by influencing the endogenous variables, were water temperature, CO_2 saturation, and DOC concentrations.

Covariance structures (indicated by the ~~ symbol) of the exogenous variables were added to the model (Eqs. (6) and (7) to represent photosynthesis and respiratory cycles that affect in-stream DO, CO_2, and DOC concentrations. To develop the best-fit SEM, the removal of the least essential (p-values > 0.05) predictor variables in the theoretical SEM was done sequentially until the model with the highest parsimony fit index (PNFI) and a root mean squared error of approximation (RMSEA) of ≤ 0.05 was reached (Schumacker and Lomax, 2010). Graphical representations of the significant relationship pathways from the best-fit models, including standardized slope parameter estimates, were done using the "semPlot" package in R version 4.3.2.

$$Ln\ N_2O\ saturation \sim DO\ saturation + Ln\ DOC + Ln\ NO_3 + Ln\ NH_4 + Ln\ CO_2\ saturation + Water\ temperature \quad (2)$$

$$Ln\ NO_3 \sim DO\ saturation + Ln\ NH_4 + Ln\ DOC + Ln\ CO_2\ saturation + Water\ temperature \quad (3)$$

$$Ln\ NH_4 \sim DO\ saturation + Ln\ DOC + Ln\ CO_2\ saturation + Water\ temperature \quad (4)$$

$$DO\ saturation \sim Ln\ DOC + Water\ temperature \quad (5)$$

$$DO\ saturation \sim\sim Ln\ CO_2\ saturation \quad (6)$$

$$Ln\ DOC \sim\sim Ln\ CO_2\ saturation \quad (7)$$

2.1.4. Monte Carlo simulations investigating the sensitivity of N_2O to CO_2 and DOC:NO_3 ratio changes

In addition to assessing the interactive effects of CO_2 saturation and DOC:NO_3 molar ratios on N_2O saturation globally, we also examined how the reported underestimation of riverine CO_2 emissions due to daytime sampling bias (Gómez-Gener et al., 2021), combined with projected future global land-use changes (e.g., forest to urban or cropland: Alexander et al., 2018; Li et al., 2019), could amplify riverine N_2O emissions. Assuming GHG saturation is proportional to flux, we first estimated the impact of the reported 27 % global average increase in riverine CO_2 emissions due to nighttime emissions by Gómez-Gener et al. (2021) on riverine N_2O emissions. Using a Monte Carlo approach for uncertainty assessment ("MASS" package in R version 4.3.2), we generated 1,000 coefficient sets from a multivariate normal distribution based on the model estimates and their covariance from the LME model

(mixed-effects model linking N_2O, CO_2, and DOC:NO_3 ratios). We then predicted N_2O saturation before and after applying a 27 % increase in riverine CO_2 saturation using the LME model, expressing the difference between the two as a percentage for each sampling date and site in the global dataset. The resulting relative % N_2O changes were summarized by calculating the median and interquartile range, and visualized using a histogram.

For the second part of the analysis, which focused on quantifying how land-use changes from forest to cropland or urban areas may affect riverine N_2O saturation, we also used the global mixed-effects model described above (LME) and applied Monte Carlo simulations to estimate uncertainty ("MASS" package in R version 4.3.2). Specifically, using the observed data from catchments dominated by forests, cropland, or urban areas as reference (Fig. S1), we generated 1,000 combinations of CO_2 and DOC:NO_3 values based on their observed global ranges in each land use class and their correlation derived from the LME model ("MASS" package in R version 4.3.2). We then predicted N_2O saturation from the 1000 new combinations in each land use class using varying model (LME) coefficients sampled from their multivariate normal distribution ("MASS" package in R version 4.3.2). The relative percentage differences in predicted N_2O saturation resulting from land use shifts (forest to cropland and forest to urban) in the generated dataset were computed and visualized in histograms, also indicating their median and interquartile range. We also applied a 27 % correction factor to account for potential nighttime CO_2 underestimation, repeating the simulation process and generating histograms with similar summary statistics.

2.2. Sediment microcosm experiment

2.2.1. Study area and sampling strategy

Microcosm stream water and sediment incubation experiments were conducted to provide process-based evidence on the biogeochemical stimulation of riverine N_2O production by CO_2 concentrations. To achieve this objective, we focused on assessing the effect of manipulated CO_2 treatments (ambient, 5000 ppm, 10000 ppm, 20000 ppm) on gross nitrification rates, N_2O saturation, net N_2O production, and functional gene abundances of nitrification and denitrification. Eight stream sites (1-3 orders; stream size classification based on (Strahler, 1952) located in two headwater catchments in Germany (Schwingbach and Loisach) were selected for this experiment (Fig. S7). The sites included two forest and two grassland sites in the Loisach catchment and two cropland and two forest sites in the Schwingbach catchment (See Mwanake et al., 2023a for extensive site details). These sites were also part of the compiled meta-data and represented the primary land use classes in the global data (Fig. S1: forests, pastures, and croplands).

The Loisach catchment is located in the mountainous region of Bavaria in southeastern Germany, with an elevation range from 616–2643 m above sea level (coordinates in decimal degrees: 47.4700, 11.0500). The catchment mainly comprises mixed forests (92 %) on the mountain slopes, pasturelands, and drained wetlands with intensively and extensively managed grasslands (8 %) at the valley bottoms. The climate is cold and temperate (Dfb, Köppen climate classification; Kottek et al., 2006), with annual precipitation of 1,693 mm (monthly mean min: 87 mm, monthly mean max: 207 mm) (1999 – 2019) and a mean annual temperature of 3.8 °C (monthly mean min: -6.6 °C, monthly mean max: 13.1 °C) (1991 – 2021) (Climate-data.org, Link). The Schwingbach catchment is located in the central-German state of Hesse, with a much lower elevation ranging from 176 – 480 m above sea level (coordinates in decimal degrees: 50.5000, 8.6100). The catchment comprises mixed land uses with ~47 % forests, ~45 % fertilized croplands, and 8 % settlement areas (Wangari et al., 2022). The climate is warm and temperate (Cfb, Köppen climate classification; Kottek et al., 2006), with an annual rainfall of 742 mm (monthly mean min: 51 mm, monthly mean max: 72 mm) (1999 – 2019) and a mean annual temperature of 9.8 °C (monthly mean min: 1.3 °C, monthly mean max: 18.8 °C) (1991 – 2021) (Climate-data.org, Link).

2.2.2. Sediment, water, and gas sampling

To mimic close-to-natural conditions in our microcosm experiments, we sampled both stream sediments and water from the eight sites on two dates in autumn (4/10/2022 and 20/10/2022). The choice of the autumn season was based on past experience from the studied sites (See Mwanake et al., 2023a). During the autumn season, the selected sites were characterized by the lowest discharge (Mwanake et al., 2023a), i.e., conditions we assumed to be associated with the highest sediment retention times due to the low flow velocities, thus providing the best timing for sediment sampling. At every site visit, sediment samples were randomly collected from ~10 locations within a 2 m reach at ~0 – 10 cm depths. The sediment sub-samples at each site were merged and filtered in the field through a 5 mm sieve to remove large stones and plant materials. The homogenized and filtered sample was placed in acid-washed plastic containers (2 L). In addition, stream water required for incubation was sampled in acid-washed plastic containers (10 L). The sediment and water samples were transported to the laboratory at Karlsruhe Institute of Technology, Campus Alpin, within 24 hours of collection for incubation.

On-site observations at the time of sampling included measurements of in-stream water temperature (°C), electrical conductivity (μS cm^{-1}), dissolved oxygen (DO) (% saturations), and pH using a Pro DSS multiprobe (YSI Inc., USA). Water samples were also collected from the stream sites in triplicates for physico-chemical analyses. The samples were filtered on-site through polyethersulfone (PES) filters (0.45 μm pore size and pre-leached with Milli-Q water) into 30 ml acid-washed HDPE bottles and stored in the refrigerator at 4 °C before being analyzed for dissolved N and C. Dissolved inorganic nitrogen (DIN) concentrations in the samples were quantified using colorimetric methods, whereby the absorbance of the samples and standards of known concentrations (0.1, 0.5, 1, 2, 3, 4, and 5 mg L^{-1} N) were measured on a microplate spectrophotometer (Model: Epoch, BioTek Inc., USA). NO_3-N concentrations were analyzed by adding Griess reagent for color formation, and the absorbance of the samples was measured at 540 nm (Patton et al., 2011). NH_4-N concentrations were analyzed using the indophenol method by measuring the absorbance of the samples at 660 nm (Bolleter et al., 1961). DOC and TDN concentrations were measured simultaneously using a DOC/ TDN analyzer (Dimatoc 2000, Dimatec, Germany).

We collected triplicate gas samples at each of the eight sites using the headspace equilibration technique (Raymond et al., 1997) to quantify *in-situ* dissolved GHG concentrations. In brief, 80 ml of stream water was equilibrated with 20 ml of atmospheric air in a syringe by shaking it in stream water for two minutes. The headspace equilibrated gas samples (17 ml) were then drawn from the syringes and stored in pre-evacuated 10 ml glass vials for later analysis in the laboratory. Atmospheric air samples were also collected at every site visit to correct for background atmospheric GHG concentrations in the headspace before equilibration. GHG concentrations in the gas samples were analyzed using an SRI gas chromatograph (8610C, Germany) with an electron capture detector (ECD) for N_2O and a flame ionization detector (FID) for CO_2 concentrations.

Dissolved CO_2 and N_2O concentrations in the stream water (C_{sw}) in moles L^{-1} were calculated based on the difference between post-equilibration gas concentrations in the headspace (C_{post_h}) in moles L^{-1} and the water (C_{post_w}) in moles L^{-1}, with the pre-equilibration gas concentrations in the headspace (C_{pre_h}) in moles L^{-1} to correct for the atmospheric concentrations that were intitialy in the headspace (Eq. (8)) (Aho and Raymond, 2019). We used the ideal gas law to calculate the headspace CO_2 and N_2O concentrations in moles L^{-1}. The water-phase CO_2 and N_2O concentrations in moles L^{-1} were calculated using Henry's Law (Eq. (9)).

$$C_{sw} = C_{post\_w} + C_{post\_h} - C_{pre\_h} \quad (8)$$

$$C_w = P \times H_s \quad (9)$$

Where C_w represents either the actual dissolved gas concentration in the stream water in moles L^{-1} or the theoretical gas concentration in the stream water if it were in equilibrium with atmospheric concentrations in moles L^{-1}, P is the partial pressure of the gas in atm (mixing ratio in ppmv from GC × atmospheric pressure), and H_s is the Henrys solubility constant for CO_2(Weiss, 1974) and N_2O (Weiss and Price, 1980) in moles L^{-1} atm^{-1}. Both concentrations were then expressed as % saturations similar to the global dataset (Eq. (1)).

2.2.3. Experimental setup

For each site, 10 g of fresh sediment and 50 ml of stream water were first added to 15 (6 for control+9 for CO_2 treatments) 140 mL glass bottles (Sigma Aldrich). 1 ml of ^{15}N- NO_3 (5000μmoles/L, ^{15}N at 99 %) was then added to each bottle for the quantification of gross nitrification rates (GNR) using the isotopic pool dilution method (Murphy et al., 2003) and the membrane inlet mass spectrometer for measurements of $^{15}NO_3$-N concentrations (Lin et al., 2021). The 6 control bottles for each site included 3 replicates for initial conditions before incubation (T_0) and 3 replicates to be sampled after incubation (T_1). All 6 control bottles were capped using gas-tight lids with rubber stoppers on the top to allow headspace gas sampling. The glass bottles were placed in the shaker at 250 rpm for mixing. After mixing on the shaker for 4 min, half of the bottles (3) were incubated in the dark for 45 h in a shaking water bath (rpm 120, 20 °C) to mimic sediment and stream water movements along natural ecosystems. The other half were destructively sampled for initial concentrations of water physico-chemical variables and dissolved GHG concentrations.

In addition to CO_2 production during incubation of the 3 control bottles with ambient headspace conditions, we manipulated CO_2 and O_2 headspace concentrations in separate sediment-slurry bottles before incubation (3 treatments of 3 replicates each = 9 bottles). These treatments mainly aimed to study the effect of CO_2 and O_2 concentration changes in water samples on N_2O production. The targeted CO_2 concentrations after the enrichment were aimed to be within the range of field measurements but sufficient to cause an effect on ammonium oxidizing communities during the short incubation period, i.e., within the optimal range of 0.0108 – 1.0426 mmol CO_2 L^{-1} for AOB growth rates (Denecke and Liebig, 2003). For the treatment, the 9 bottles were first capped using gas-tight lids with rubber stoppers on the top. We then manipulated the headspace concentrations in the bottles by replacing the ambient air (~ 20 % O_2 and 410 ppm CO_2) in the 80ml headspace with different volumes of 20000 ppm CO_2 in a helium atmosphere. The final three headspace treatments were 5000 ppm of CO_2 and 15 % of O_2, 10000 ppm of CO_2 and 10 % of O_2, and 20000 ppm of CO_2 and 0 % of O_2. The rationale for decreasing headspace O_2 while increasing CO_2 concentrations was to mimic respiration and avoid creating artificial experimental artifacts, i.e., constant O_2 at elevated CO_2 conditions. These 9 treatment bottles were incubated simultaneously in the dark and under conditions similar to the 3 (T_1) control bottles.

2.2.4. Measurement of dissolved gases

Sampling initial (T_0) and final (T_1) concentrations of dissolved gasses involved taking duplicate samples from each bottle's headspace before opening the gas-tight lids. The headspace concentrations of CO_2 and N_2O were measured on a gas chromatograph (SRI, 8610C, Germany). These concentrations were then converted to dissolved concentrations in the aqueous phase using the ideal gas law and Henry's law described above for the in-situ samples and then expressed as % saturations. After gas sampling, the bottles were opened, and 0.2 ml of saturated $ZnCl_2$ solution was added to each bottle to stop the microbial activity. 30 ml of the sediment-slurry was gently transferred to pre-washed plastic beakers for the initial and final DO and pH measurements using a Pro DSS multiprobe (YSI Inc., USA).

2.2.5. Measurement of dissolved inorganic nitrogen

Initial (T_0) and final (T_1) concentrations of DIN in the slurry mixtures were measured by transferring 10 ml of the remaining slurry to 50 ml centrifuge tubes and adding 40 ml of 1 M KCl to the slurry mixture to extract the DIN. During extraction, the KCL and the slurry mixtures were shaken for 1 h at 250 rpm. The mixtures were then allowed to decant, and the upper waters were filtered through a 0.45 μm pore-size PES filter for later analyses of $^{15}NO_3$-N, total NH_4-N, and total NO_3-N concentrations in the filtrates. From the extracts, total NH_4-N and NO_3-N concentrations were analyzed using the colorimetric method described above, and DOC was analyzed using a Dimatoc 2000 (Dimatec, Germany). The initial and final $^{15}NO_3$-N in the extracts were then analyzed on the membrane inlet mass spectrometer (MIMS) using the REOX/MIMS method (Lin et al., 2021).

2.2.6. Measurement of $^{15}NO_3$-N using the (REOX/MIMS) method

The REOX (REduction-OXidation)/MIMS method is both sensitive (~0.1 μM) and also precise (relative standard deviation = 0.1– 4.37 %) in quantifying $^{15}NO_3$-N concentrations in liquid samples with a wide range of concentrations (0.1- 500 μM) and salinities (0–35 ‰) (Kana et al., 1994; Lin et al., 2021). To quantify the $^{15}NO_3$-N in our extract samples, we transferred 15 ml of the extract to 50 ml centrifuge tubes. About 250 mg of zinc powder and 75 μL of H_2SO_4 were added to each sample, and the centrifuge tubes were placed in the shaker (250 rpm at room temperature) for 30 min. During the mixing, the $^{15}NO_3$-N in our samples was reduced to $^{15}NH_4$-N by the zinc powder in the acidic medium. The liquid phase of the mixtures was then gently transferred into 12 ml borosilicate glass vials (Labco) until they brimmed, and the vials were tightly capped with gas-tight septum caps. The next step entailed oxidizing $^{15}NH_4$-N in the samples to dissolved N_2 isotopes ($^{29}N_2$ and $^{30}N_2$) by adding 250 μL of oxidant solution (hypobromite iodine). The oxidation solution was gently added through the septum of the 12 ml Borosilicate glass vials using a needle to prevent the formed N_2 gas from escaping to the atmosphere.

The N_2 isotopes in the samples were then immediately quantified using the MIMS (Bay Instruments, Easton, MD, USA). The MIMS measurements involved continuous uptake of the liquid (extract) samples through a gas-permeable silicone membrane using a peristaltic pump and detecting N_2 isotopes on a quadrupole mass analyzer (Pfeiffer vacuum PrismaPlus). The N_2 isotopes were then drawn from the liquid phase by diffusion through the membrane to the mass spectrometer in a high vacuum environment. We developed a calibration curve of known $^{15}NO_3$-N concentrations and the ($^{29}N_2$/Ar)/2 + $^{30}N_2$/Ar) current ratios quantified on the MIMS (Fig. S8). The MIMS setup included a liquid N_2 trap and a reduction furnace to minimize water vapor and other dissolved gas interferences on the N_2 isotope measurements (Kana et al., 1994).

2.2.7. Quantification of potential gross nitrification and net N_2O fluxes

The isotopic pool dilution method was used to quantify the sediment and water-column potential gross nitrification rates (pGNR) (Murphy et al., 2003). For the calculation, we used the initial (T_0) and the final (T_1) $^{15}NO_3$-N and total NO_3-N values measured in the extracts from the initial (T_0) and final (T_1) bottles (Eq. (10)).

$$pGNR = \frac{M_i - M_f}{t} \times \frac{\log\left(\frac{H_i \times M_f}{H_f \times M_i}\right)}{\log\left(\frac{M_i}{M_f}\right)} \quad (10)$$

In the equation above, pGNR is the respective rate of gross nitrification in μg N g^{-1} d^{-1}, M_i and M_f are the individual concentrations of total NO_3-N in initial and final sediment-slurries in μg N g^{-1}, H_i and H_f are the respective concentrations of $^{15}NO_3$-N in initial and final sediment in μg N g^{-1}, and t is the incubation time in days (Murphy et al., 2003).

The net N_2O fluxes during the incubations were calculated using Eq. (11), where FN_2O is the N_2O fluxes in ng g^{-1} d^{-1}, C_i and C_f are the respective concentrations of N_2O in initial and final sediment-slurries in

ng g^{-1}, and t is the incubation time in days. pGNRs and net N_2O production rates were then expressed in grams of dry sediment weight (g-SDW) after correcting for the moisture content in the sampled sediment. The moisture content was determined by drying 20 g of wet sediment in an oven at 105 °C for 24 h.

$$FN_2O = \frac{C_f - C_i}{t} \quad (11)$$

2.2.8. Quantification of functional gene abundances for nitrification and denitrification

About 1 g of sediment-slurry was sampled from the remaining slurry in each bottle after incubation to analyze the abundance of marker genes representing nitrification and denitrification processes using extracted DNA and quantitative real-time polymerase chain reaction (qPCR) (Banerjee and Siciliano, 2012). Therefore, the slurry samples were stored in sterile 1.5 ml Eppendorf tubes, frozen in liquid nitrogen, and then transferred to a deep freezer at -80 °C for later analysis (Banerjee and Siciliano, 2012). Sediment DNA samples were taken from each replicate sample of the ambient bottles and the three levels of CO_2 treatments. The DNA was extracted using the NucleoSpin Soil kit (Macherey Nagel), and yield and purity were checked with a spectrophotometer (Nanodrop, PeqLab, Germany). Following an SYBR-Green®-based (Applied Biosystems) approach with a 7300 real-time qPCR machine (Thermo Fisher Scientific, Darmstadt, Germany), qPCR runs were performed to quantify the abundance of indicator genes for ammonium oxidation (ammonia oxidization by archaea (*amoA* AOA), ammonia oxidization by bacteria (*amoB* AOB) and denitrification (*nirS, nirK*, and clade I *nosZ*). Previous research showed that the other nosZ clades were not responsive to nitrification changes, so only clade I was selected for the experiment (Duffner et al., 2021). The optimal dilution rate of the DNA extracts was fixed to 1:16 after testing for PCR inhibition. PCR reaction mixtures (25 µL) contained 12.5 µL of SYBR Green PCR Master Mix (Thermo Fisher Scientific, Darmstadt, Germany), 10 pmol of each primer, 8.5 µL of DEPC water, and 2 µL of DNA template. 2 µL of DEPC water and the mentioned reagents were used to constitute the assay negatives (no template). Serial dilutions of plasmid DNA containing the PCR products of the genes of interest (Table S2) were used to prepare the standard curves. The abundance of each marker gene was then expressed in units of copies per gram of dry sediment weight (g-SDW^{-1}). Quality was checked with electrophoreses in 1 % (w/v) agarose gels, and the dissociation-curve analysis was performed with the 7300 System SDS Software v1.3.0 (Applied Biosystems).

2.2.9. Statistical analyses

We used linear regression models on the experimental data from the eight sites to determine biogeochemical links between CO_2 oversaturation and N_2O production from nitrification-driven processes. In the models, the relationships of CO_2 concentrations against several parameters such as GNR, N_2O production rates, and the marker genes of ammonium oxidation (AOA and AOB) and nitrite (*nirS* and *nirK*) and N_2O (*nosZ*) reducers were explored. Because we hypothesized that nitrification would be dominant when DOC:NO_3 ratios are relatively low, we also examined the interaction of CO_2 and DOC:NO_3 ratios on nitrification, denitrification, and N_2O-related parameters. Similar to the meta-analysis, forest plots were used to visualize the standardized effect sizes of the fixed effects from the models ("sjPlot" and "ggplot2" packages in R version 4.3.2). To visualize the CO_2 * DOC:NO_3 interaction effects predicted from the regression models, multiple (n=10) parameter-CO_2 slope ± SE values were generated ("interactions" package in R version 4.3.2), and their bivariate relationships with changing DOC:NO_3 ratios were analyzed. Before model construction and evaluation, CO_2 and DOC:NO_3 and some independent variables were always transformed using the natural logarithm to meet the normality assumption.

3. Results

3.1. Global meta-analysis

3.1.1. Effect of in-stream CO_2 on N_2O saturation values along DOC:NO_3 ratios gradients

In-stream N_2O and CO_2 concentrations in the global dataset were mainly over-saturated (median; 407 % for CO_2 and median; 162 % for N_2O) relative to riverine concentrations in equilibrium with the atmosphere (CO_2: 421 ppm and N_2O: 0.33 ppm). The saturation levels of both gases also varied widely, spanning over 4 orders of magnitude (1– 54452 % for N_2O and 3– 23495 % for CO_2) (N). Similar to N_2O and CO_2 saturations, DOC:NO_3 ratios in global fluvial ecosystems were also highly variable, ranging from 0.055 – 16985. In terms of land-use influences, N_2O and CO_2 saturations were significantly (p-value < 0.05; Wilcoxon signed-rank test) higher in human-influenced cropland and urban-dominated catchments compared to forested catchments (Fig. S1). In contrast, DOC:NO_3 trends mostly followed opposite trends and were higher in forested catchments than in cropland and urban-dominated catchments (Fig. S1).

Based on the results from a linear mixed effect model, CO_2 saturation, DOC:NO_3 molar ratios, and their interaction had significant correlations with in-stream N_2O saturation (p-value<0.001, r^2=0.71; Fig. S2). Increases in CO_2 saturation led to a substantial log-linear positive response in riverine N_2O saturation (effect size = 0.50, p-value<0.001). In contrast to CO_2 effects, increases in DOC:NO_3 ratios resulted in log-linear declines in N_2O saturation (effect size = -0.25 p-value<0.001; Fig. S2). The increase in DOC:NO_3 ratios also led to declines in the positive response of N_2O saturation to CO_2 saturation, with a significant negative slope at the highest DOC:NO_3 ratios (interactive effect size = -0.23; Fig. S2; Fig. 1).

The results from a multivariate structural equation model (SEM) also showed significant interactions among the direct and indirect drivers of N_2O saturation in the global data (p <0.05; Fig. 2, Table S2). From the standardized slope parameter estimates, DOC and CO_2 positively covaried and were negatively related to DO saturations. While DOC concentrations were positively related to NH_4-N concentrations, CO_2 saturation showed trends of a negative relationship with NH_4-N (not significant) and was additionally positively related to NO_3-N concentrations (Fig. 2). DO and NH_4-N concentrations had positive relationships with NO_3-N concentrations, whereby increase in DO and NH_4-N resulted in an up to 30 % increase in NO_3-N concentrations (Fig. 2). Direct relationships between N_2O and either CO_2 or DOC differed in magnitude and direction. An increase in CO_2 resulted in a 56 % increase in N_2O saturation. However, DOC increases had contrasting effects on N_2O, resulting in an 8 % decrease in N_2O saturation (Fig. 2). N_2O saturation was also positively related to DO and NO_3-N concentrations (Fig. 2).

3.1.2. Effect of in-vitro CO_2 enrichment on nitrification and net N_2O production

In our lab experiments, increasing CO_2 saturation was positively correlated to nitrification and N_2O-related parameters, but the relationships decreased in magnitude with increasing DOC:NO_3 ratios similar to the global dataset (Fig. 3). Within our eight experimental sites, background stream water DIN, DOC, N_2O saturation, CO_2 saturation and the DOC:NO_3 ratios ranged from 52 – 87 µmol L^{-1}, 87 – 402 µmol L^{-1}, 9 – 492 %, 196 – 1450 %, and 1.37 – 9.97, respectively. CO_2 enrichment during the sediment-slurry incubation experiments resulted in final CO_2 saturation values ranging from 498 – 4774 %, which were within the range of the global dataset and the reported range for optimum nitrifier growth rates (Denecke and Liebig, 2003).

Increases in *in-vitro* CO_2 saturation were positively related to increases in sediment-slurry potential gross nitrification rates (pGNRs) and the gene abundance of AOA and AOB ammonium oxidizers (effect size 0.39 – 0.47, p-value<0.001; Fig. 3 A, B). The increase in CO_2

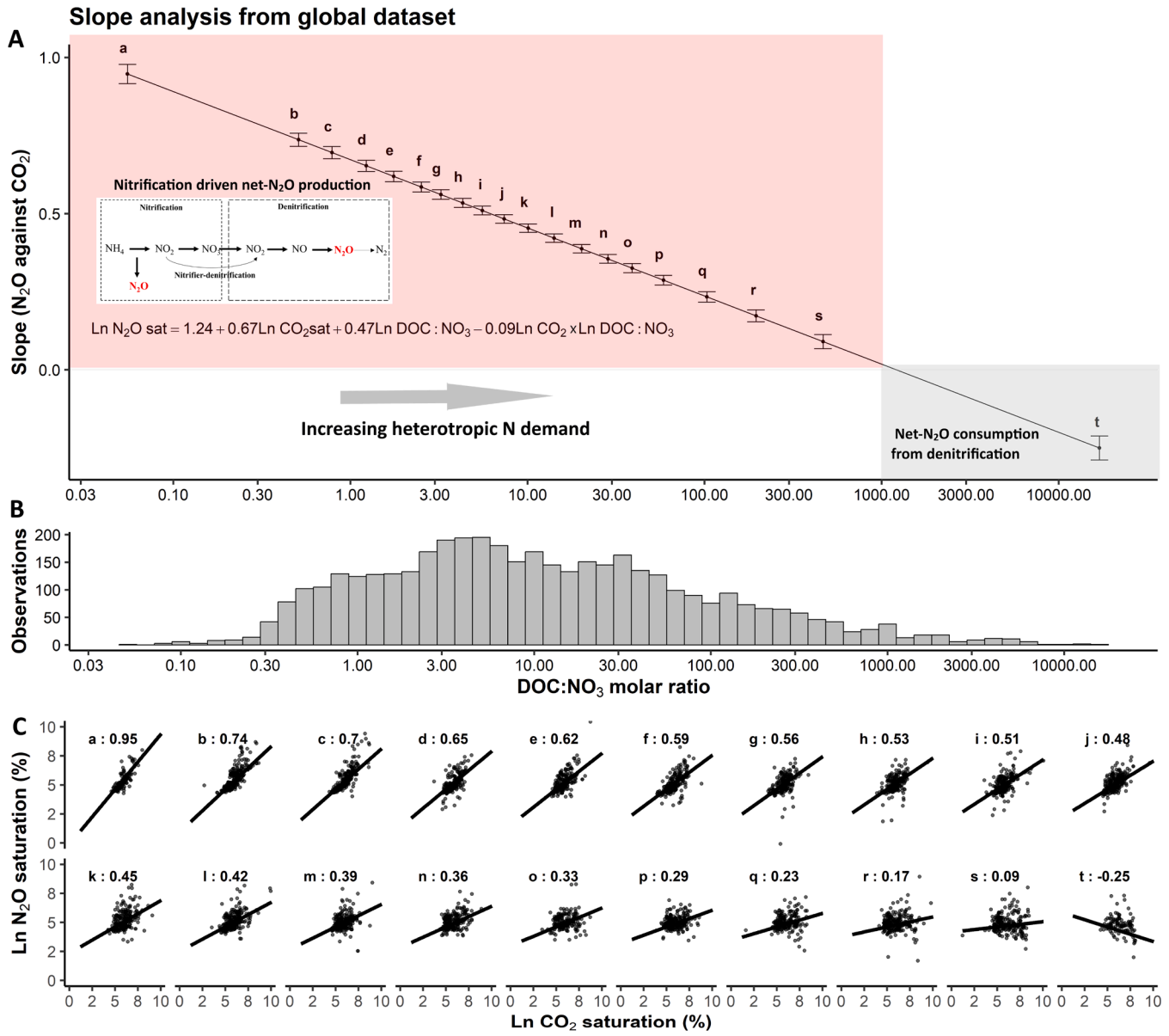

Fig. 1. A) Interaction plot from the linear mixed effect model (Fig. S2) illustrating the predicted non-linear decline in the slopes (p-value<0.01; n= 20) between N_2O and CO_2 saturation levels (y-axis) with increasing DOC:NO_3 ratios (x-axis in log scale) in the global data. The equation on the plot outlines the log-linear relationship of the three parameters from the linear mixed-effects model (Fig. S2). The red shaded area, where the slopes are significantly positive, potentially indicates nitrification-driven N_2O production, while the grey shaded area, where slopes are significantly negative, indicates N_2O consumption from complete denitrification. The grey arrow shows increasing heterotrophic N demand with increasing DOC:NO_3 ratios proposed by Taylor and Townsend, 2010. Error bars on the slopes represent ± SE values. **B)** Histogram showing the distribution of DOC:NO_3 ratios in the global data (N=4158). **C)** N_2O-CO_2 scatterplots of actual field data with predicted slopes (black regression lines) across increasing DOC:NO_3 ratios. The predicted slopes also correspond to each slope in A, as indicated by matching lowercase letters.

saturation was also positively related to increases in N_2O saturation and net N_2O fluxes (effect size = 0.24 – 0.36, p-value<0.05; Fig. 3 C, E). However, these positive relationships with CO_2 gradually decreased in magnitude with increases in DOC:NO_3 ratios (interactive effect size = -0.26 – -0.39, p-value<0.05) and were insignificant at sites with DOC:NO_3 ratios > 5 characterized by low upstream agricultural areas (Fig. 4). Potential gross nitrification rates were positively related to *in-vitro* N_2O saturation levels (effect size 0.43, p-value<0.001; Fig S3A), but this relationship was also not significant above a DOC:NO_3 molar ratio of 5 (Fig. S3B). In contrast to CO_2, N_2O and nitrification-related parameters mainly had negative relationships with O_2 and pH (Fig. S4). Denitrification potential, as indicated by the gene abundances of denitrifiers (nirS, nirK, and clade I nosZ), showed increases with DOC:NO_3 ratios (effect size = 0.30 - 0.58, p-value<0.001, Figs. 3 D, F, 4), opposite to what was found for N_2O and nitrification related parameters. We also found that the denitrifier gene abundances mainly showed substantial positive relationships with AOB (effect size = 0.64 – 0.72, p-value<0.001), while similar relationships with AOA were not significant (Fig. S5). Overall, the relative gene abundance of ammonium oxidizers compared to denitrifiers, was significantly positively related to N_2O saturation and negatively related to DOC:NO_3 ratios (Fig. S6).

4. Discussion

Here, results from the meta-analysis and the experimental approach suggest a possible CO_2 fertilization effect on nitrogen cycling processes

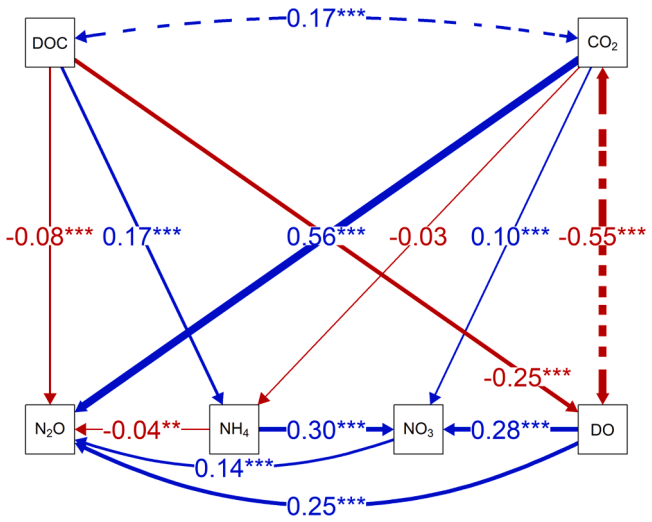

Fig. 2. Results from a structural equation model (SEM, Table S2) showing relationships between N_2O saturation and DOC (μmol L^{-1}), CO_2 (% saturation), DO (% saturation), NH_4-N (μmol L^{-1}) and NO_3-N (μmol L^{-1}) concentrations from the global dataset. Numbers show standardized slopes; blue colors represent positive relationships, and red represents negative relationships. The thickness of the line shows the strength of the relationship, and the number of asterisks represents the level of significance with *p<0.05, ** p<0.01, and *** p<0.001. Dashed lines indicate significant covariances in the SEM. All variables were LN transformed except for DO saturation.

responsible for net N_2O production in rivers (ammonium oxidation, nitrifier denitrification, and coupled nitrification-denitrification), which may account for the positive relationship between CO_2 and N_2O saturation values observed in most global fluvial ecosystems (Fig. 1). However, the positive effect of CO_2 fertilization on riverine N_2O production diminished at elevated DOC:NO_3 ratios, indicating that under those conditions, nitrification (a precursor process to increased N_2O production also from denitrification) may be hindered due to heightened heterotrophic NH_4 competition and oxygen limitation. (See Helton et al., 2015; Taylor and Townsend, 2010). The possible importance of nitrification in driving net N_2O production shown in this study is also consistent with a review of the results from the second Lotic Intersite Nitrogen eXperiments (LINX II; Beaulieu et al., 2011) on the controls of N_2O yields from fluvial ecosystems (Winnick, 2021). In that study, N_2O yields were negatively correlated with denitrification efficiencies and positively correlated with ammonium concentrations. This finding suggests that nitrification, which has been shown to result in higher N_2O yields due to oxygen inhibition of N_2O reduction (Meyer et al., 2008), may induce net fluvial N_2O production relative to denitrification. Wannick's (2021) findings were further corroborated in a recent study of global agricultural headwater streams, which found that ammonia-derived pathways accounted for the majority of N_2O sources in these ecosystems rather than nitrate-derived pathways (S. Wang et al., 2024).

Our study complements these studies by providing mechanistic insights into the factors driving nitrification-driven net N_2O production in global fluvial ecosystems and the potential positive climate feedback between two key greenhouse gases. As a summary of our key findings discussed in detail below, we show that nitrification-induced net-N_2O production is possibly linked to the balance between CO_2 concentrations and the DOC:NO_3 ratios, which are both influenced by anthropogenic activities (Fig. 5). In human-influenced fluvial ecosystems such as those within agricultural and urban areas, combined conditions of low DOC:NO_3 ratios and CO_2 oversaturation in them will favor net-N_2O production from enhanced nitrification rates. However, in more natural forested ecosystems with higher DOC:NO_3 ratios and lower CO_2 saturation, nitrification rates are lower, and N_2O consumption from heterotrophic denitrification is favored (Fig. 5; Fig. S1).

4.1. The potential role of nitrification in driving the positive CO_2-N_2O relationships

Our results showed that CO_2 saturation was mainly positively related to N_2O saturation in global rivers (Fig. 1). Such a positive relationship may reflect either biogeochemical interactions between the two GHGs, as hypothesized in this study, similarities in their external sources, or a combination of both. For instance, substantial evidence that direct terrestrial inputs, particularly from urban wastewater and agricultural runoff, significantly contribute to the simultaneous loading of both N_2O and CO_2 in rivers (e.g., Mwanake et al., 2019, 2023a; W. Zhang et al., 2021). These externally sourced N_2O inputs bypass in-stream biogeochemical cycling and, therefore, do not interact with CO_2-driven N_2O production suggested in this study. To evaluate the role of biogeochemical interactions in explaining the observed positive relationship, we further investigated how this relationship varied with changing DOC:NO_3 ratios, which are known to influence nitrogen biogeochemical processes responsible for N_2O production in streams (Taylor and Townsend, 2010).

Our findings indicated that the positive effect of in-stream CO_2 on riverine N_2O saturation significantly declined with increasing DOC:NO_3 ratios, suggesting an important role of biogeochemical linkages between the two GHGs in shaping this relationship (Fig. 1). To explore how CO_2 may enhance N_2O production at low DOC:NO_3 ratios, we examined its potential role as a carbon source stimulating nitrification, a mechanism previously observed in wastewater treatment research (Jiang et al., 2015). These enhanced nitrification rates would also provide the nitrate required for N_2O production from incomplete denitrification (Cébron et al., 2005), explaining the overall net positive effect of CO_2 on N_2O in rivers. Based on the multivariate analysis, we found positive relationships of CO_2 with N_2O and NO_3 and its inverse relationship with NH_4, which suggested that the CO_2 fertilization effect on net N_2O production was possibly linked to nitrification (Fig. 2). The possible occurrence of nitrification in the global data was further supported by the positive relationships of DO and NH_4 concentrations with NO_3, as previous studies have shown that elevated oxygen and ammonium levels can promote riverine nitrification (Bernhardt and Likens, 2002; Kemp and Dodds, 2002; Webster et al., 2003). However, the positive relationship between NO_3 and N_2O may still imply that N_2O production is solely dominated by denitrification (e.g., Baulch et al., 2011; Beaulieu et al., 2011; Herreid et al., 2021), and we, therefore, required additional evidence linking net N_2O production to N cycling processes driven by increased nitrification rates. This evidence was drawn from our study's meta-analysis and incubation experiments. From the metanalysis, we observed a negative effect of DOC, the primary carbon source for heterotrophic denitrification, on N_2O saturation in rivers, while CO_2, the primary carbon source for nitrifiers, showed strong positive relationships with N_2O saturation (Fig. 2). This finding suggested that while CO_2-driven nitrification may be responsible for net N_2O production, conditions favoring denitrification may result to both N_2O production and consumption, as increased heterotrophic N demand under elevated DOC concentrations may lead to N_2O reduction to N_2 through complete denitrification (Quick et al., 2019).

Our incubation experiments provided further empirical evidence for the role of nitrification in driving net N_2O production in rivers, based on the availability of its primary carbon source, CO_2. At streams with DOC:NO_3 ratios <5, mainly located within agricultural areas, the experimental results supported the circumstantial evidence from the global data, showing that sediment and water column potential gross nitrification rates, the abundance of ammonium oxidizers, N_2O saturation, and net N_2O production rates increased with elevated CO_2 (Figs. 3 and 4). N_2O saturation levels at these sites were also positively related to the potential gross nitrification rates (Fig. S3). Overall, the experimental and meta-analysis findings both suggested that increased nitrification

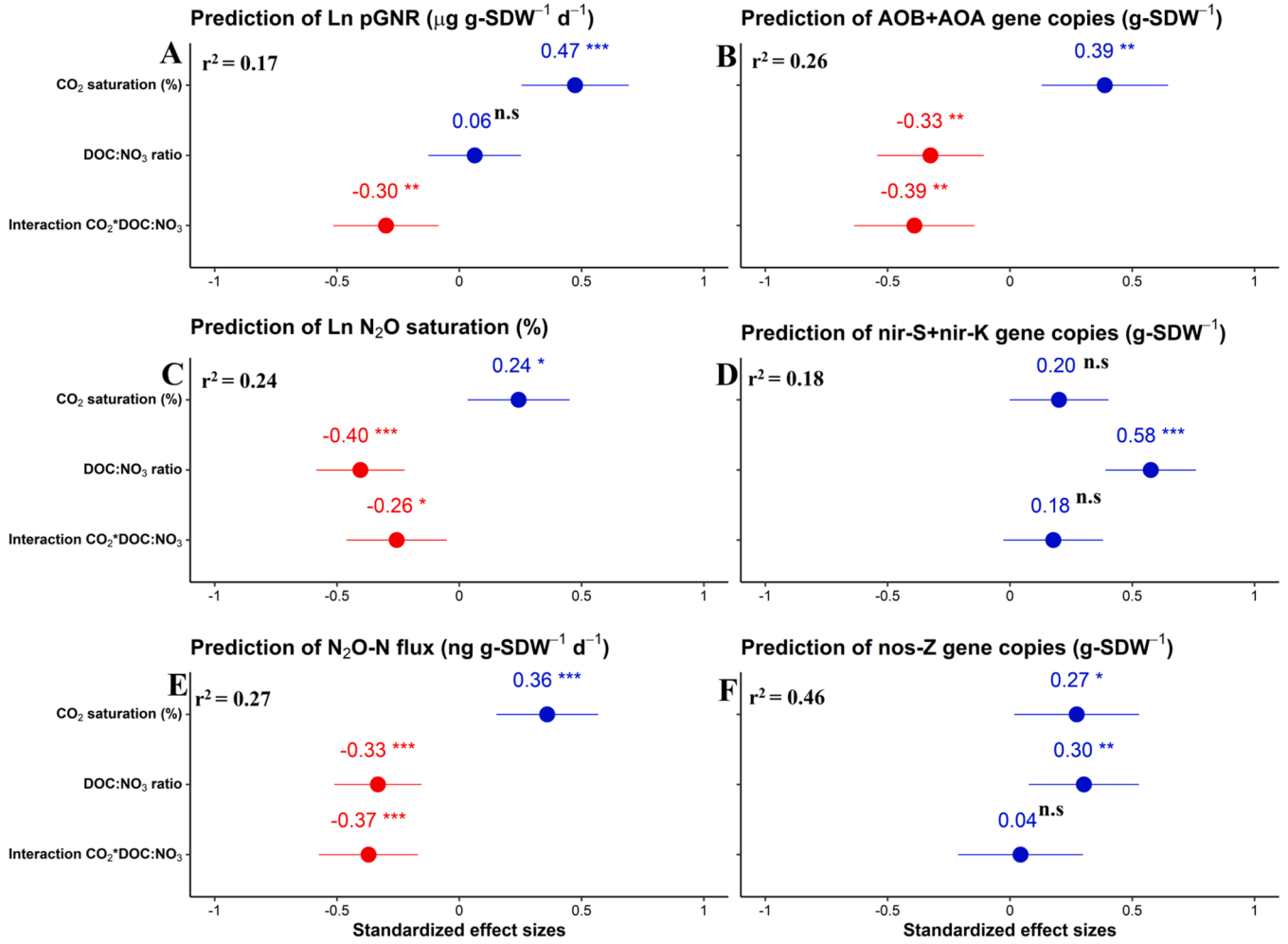

Fig. 3. Forest plots showing effect sizes from the experimental data where CO_2 saturation was manipulated in sediment slurries from 4 forested, 2 pasture, and 2 cropland-dominated streams, which varied with respect to background DOC:NO_3 ratio (see experimental setup, methods). Effect sizes of CO_2, DOC:NO_3 ratios and their interactions are shown for **A)** potential gross nitrification rates; **B)** gene abundance for ammonium oxidizers (amoA AOA; amoB AOB); **C)** N_2O % saturations; **D)** gene abundances of nitrite reducers (*nirS* and *nirK*); **E)** net N_2O production rates; and **F)** gene abundance of nitrous oxide reducers (clade I *nosZ*). Numbers show the standardized slope values from linear regression models, with blue showing positive and red showing negative relationships. Horizontal lines on the dots represent the confidence interval of the effect sizes (CI=95 %). Significance is shown by the number of asterisks *p<0.05, **p<0.01, ***p<0.001.

rates induce net N_2O production under low DOC:NO_3 ratios and high CO_2 saturation, which mainly characterizes human-influenced rivers (Fig. 5). However, the positive effects of CO_2 oversaturation on net N_2O production declined with increasing DOC:NO_3 ratios, similar to what we found in the global data (Fig. 1). We attribute this finding to reducing redox conditions and increased heterotrophic N demand under elevated DOC:NO_3 ratios (e.g., Helton et al., 2015; Taylor and Townsend, 2010), which support N_2O consumption by complete denitrification rather than its production from nitrification or incomplete denitrification. This conclusion also aligns well with the antagonistic relationship we observed between DOC:NO_3 ratios and the relative gene abundance of ammonium oxidizers compared to denitrifiers (nirS, nirK, and clade I nosZ), which was positively correlated with N_2O saturation (Fig. S6). Our findings, therefore, align with previous fluvial studies reporting overall higher N_2O yields from nitrification than from denitrification, likely due to the latter's role in also facilitating N_2O reduction under certain environmental conditions (S. Wang et al., 2024; Winnick, 2021). The dual role of denitrification was also shown in a recent global meta-analysis investigating the drivers of N_2O emission factors from rivers, where total N_2O yields from denitrification were significantly negatively correlated with DOC:NO_3 ratios (J. Wang et al., 2022). The authors attributed this negative correlation to the fact that labile carbon promotes both N_2O production and reduction via denitrification; however, the direction of this relationship depends on the nitrogen status of the riverine ecosystem (Quick et al., 2019). In nitrogen-limited riverine ecosystems, particularly in forested catchments, complete denitrification may result in rivers acting as net N_2O sinks (e.g., Aho et al., 2023; Borges et al., 2019; Mwanake et al., 2025). For instance, this mechanism has been inferred in tropical forest streams in South America and Africa, where high DOC concentrations and reducing redox conditions likely promote N_2O undersaturation through its conversion to N_2 via complete denitrification(Borges et al., 2019; Chiriboga and Borges, 2023). In contrast, nitrogen-rich riverine ecosystems, such as those in urban areas, often exhibit net N_2O production as a result of incomplete denitrification (e.g., Chen et al., 2025; C. Wang et al., 2024).

Although CO_2 oversaturation showed no significant positive effect on potential gross nitrification and N_2O production at sites with >5 DOC:NO_3 ratios, we did find a positive effect of CO_2 on the abundance of denitrification genes (Fig. 3). We contend that the stimulation of ammonium oxidizers by CO_2, particularly AOB that showed the most substantial positive relationship with the abundance of denitrifier genes (*nirS, nirK*, and clade I *nosZ*) (Fig. S5), may explain our findings. AOB may be more sensitive to increasing in-stream CO_2 concentrations than AOA as it cannot directly fix the more abundant inorganic carbon form (HCO_3^-) and is known to conduct denitrification under reducing redox conditions (Cooper et al., 1969). These results are consistent with

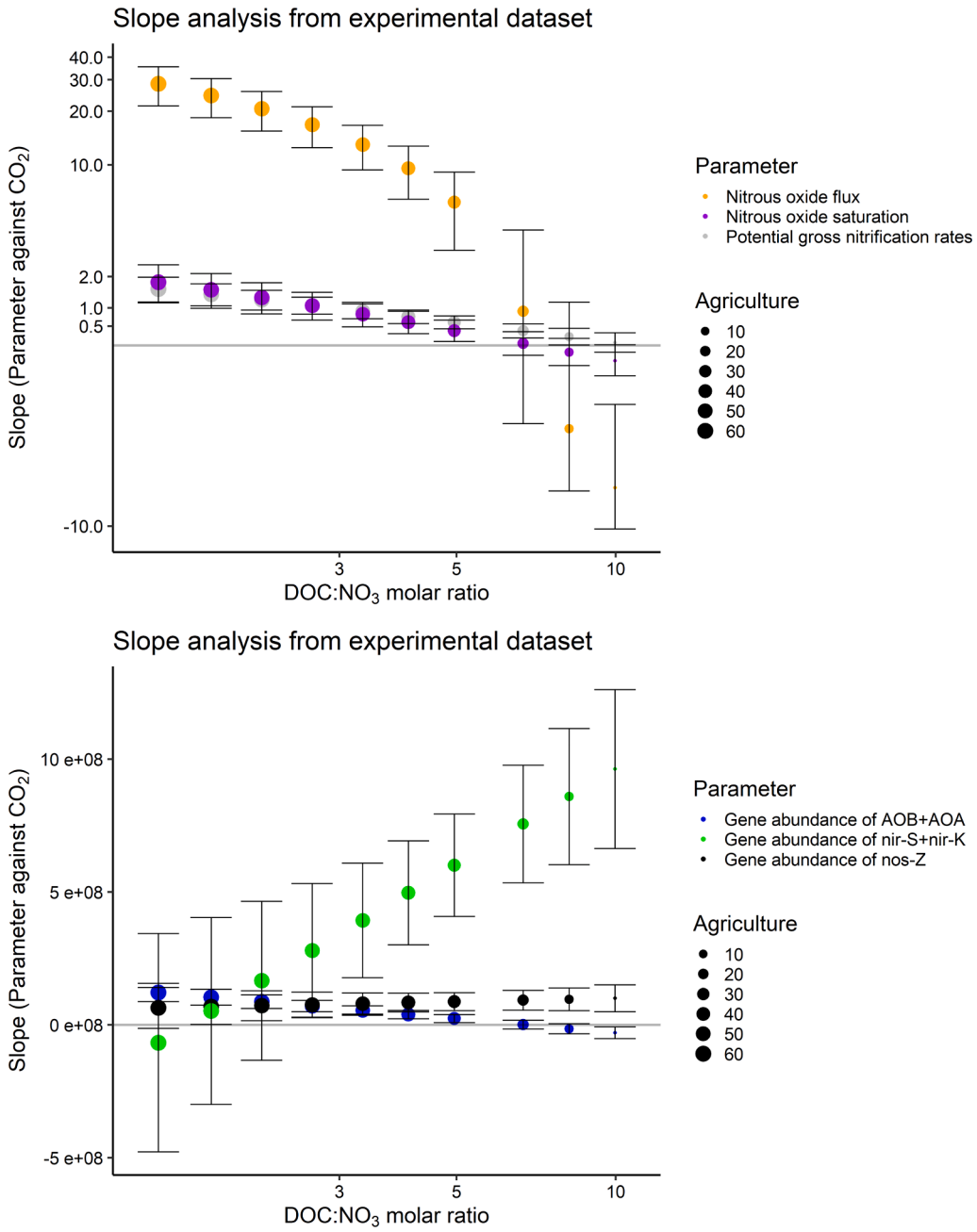

Fig. 4. Interaction plot showing model results from the experimental data set (Fig. 3) relating the slopes between several parameters and CO_2 saturation (y-axis) against DOC:NO_3 ratios (x-axis in log scale). The y-axis shows the slopes of process rates (Panel A) and gene abundances (Panel B). Error bars represent ± SE values (n= 10) along increasing DOC:NO_3 ratios. The size of the dots indicates the percent of the sub-catchment that comprises agricultural land use.

previous laboratory tracer studies, which demonstrated the existence of nitrifier denitrification by AOB (Jung et al., 2014; Stieglmeier et al., 2014; Wrage-Mönnig et al., 2018). Similar findings were also recorded in agricultural headwater streams in China, whereby metagenome-assembled genomes (MAGs) analyses indicated that nitrifying bacteria, including AOB, contain greater abundances of N_2O production-related genes than denitrifying bacteria (S. Wang et al., 2024). Based on these findings, we contend that enhanced nitrification rates from CO_2 fertilization may increase the dominance of nitrification over denitrification on net N_2O fluxes due to additional N_2O yields from AOB-mediated nitrifier denitrification.

4.2. *Disentangling CO_2 effects from covariates such as O_2 and pH*

Even though previous studies have also found that increased respiration can lead to increased N_2O fluxes from rivers (e.g., Beaulieu et al., 2011; Madinger and Hall, 2019; Reisinger et al., 2016), most of them have linked it to oxygen depletion during the process that favors N_2O production via denitrification (e.g., Rosamond et al., 2012). Our study's results offer an alternative explanatory mechanism, as CO_2 saturation, a product of respiration, showed more meaningful biogeochemical stimulations of N_2O production than O_2 and even pH (Fig. S4). In all eight experimental sites, we found either negative relationships between gross nitrification rates and the gene abundances of ammonium oxidizers with O_2 and pH or no relationships (Fig. S4). These relationships contradict the expected positive relationships with both variables, as nitrification is

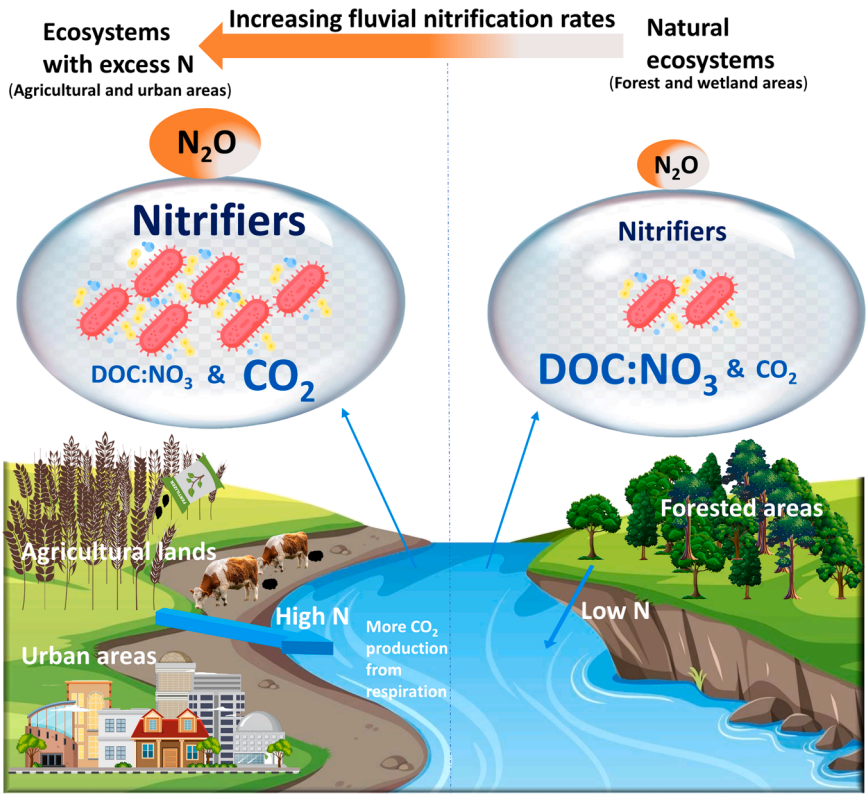

Fig. 5. Conceptual diagram outlining the mechanism of how relatively high in-stream CO_2 concentrations and low DOC:NO_3 ratios due to human activities result in enhanced nitrification-driven N_2O production in fluvial ecosystems (see Fig. S1). The size of the text indicates the magnitude of change in each parameter due to anthropogenic activities. The color gradient for in-stream N_2O concentration estimates the contribution of nitrification (red) relative to denitrification (grey) inferred from gene abundance trends in this study (Fig. S6) and the results of Wang et al. (2024).

an aerobic process known to increase with pH (e.g., Bernhardt and Likens, 2002; Huesemann et al., 2002). Based on these findings, CO_2 fertilization of ammonium oxidation and the complete nitrification process offered an alternative argument in explaining our results. Even at streams with relatively high DOC:NO_3 ratios, where heterotrophic denitrifiers may dominate due to stoichiometric advantages and reduced redox conditions, CO_2 saturation showed more substantial positive effects on the abundances of functional denitrification genes than O_2 (Fig. 4, S4). This result further suggests that improved nitrite/nitrate production with elevated CO_2 rather than declines in O_2 concentrations may also drive N_2O production from the nitrifier denitrification processes carried out by AOB or denitrifiers.

4.3. Possible implications of the CO_2 effect on global riverine N_2O emissions

Recent research indicates that unaccounted global night-time riverine CO_2 emissions are, on average, 27 % higher than daytime emissions, with the most significant differences (median: ~40 %) occurring in open-canopy streams with low DOC concentrations (Gómez-Gener et al., 2021), typical of cropland and urban streams that are known N_2O hotspots (e.g., Mwanake et al., 2025; Mwanake et al., 2023a; Xu et al., 2024). Using the log-linear biogeochemical relationship derived from the global dataset (Fig. 1A) and Monte Carlo simulations for uncertainty assessment (n=1000), we evaluated the potential impact of elevated nighttime CO_2 on riverine N_2O emissions in these streams at varying levels of DOC:NO_3 ratios. Given the positive relationship between greenhouse gas saturation and emissions, accounting for underestimated nighttime CO_2 emissions suggests that global N_2O emissions from streams could be 12 % (Interquartile range: 8 – 15) higher than current estimates. Although similar underestimations of riverine N_2O fluxes have been reported in site-specific studies (e.g., Piatka et al., 2024; Woodrow et al., 2024), this study uniquely highlights their potential significance on a global scale.

Additionally, our study suggests that the CO_2 fertilization effect on global riverine N_2O production could become a significant climate feedback mechanism with land use changes. This is because projections of global land use changes under different climate scenarios indicate substantial expansion of fertilizer-intensive croplands and urban areas by the end of the 21st century (e.g., Alexander et al., 2018; Li et al., 2019). Conceptually, this expansion is expected to lower in-stream DOC:NO_3 ratios and increase CO_2 concentrations, creating favorable conditions for high N_2O production rates from nitrification-driven processes (Fig. 5). Several studies have already shown that increased nitrogen inputs into rivers from cropland or urban-dominated catchments lower riverine C: N ratios (Wachholz et al., 2023), increase in-stream CO_2 concentrations (Xu et al., 2024), and result in higher contributions of nitrification to net N_2O production than denitrification (S. Wang et al., 2024). To calculate the potential impacts of land-use transitions on in-stream CO_2 and DOC:NO_3 dynamics and their subsequent effects on riverine N_2O emissions, we also applied the log-linear biogeochemical relationship generated in this study (Fig. 1A) and used Monte Carlo simulations (n=1000) for uncertainty assessment. For instance, using the land use-specific global range values of CO_2 saturation and DOC:NO_3 ratios (Fig. S1), a transition from forested catchments to cropland-dominated catchments results in a 45 % (IQR= -4 – 124) increase in riverine N_2O emissions. A more pronounced increase of 111 % (IQR= 18 – 297) in N_2O emissions is anticipated with shifts toward urban-dominated catchments characterized by higher CO_2 saturations and lower DOC:NO_3 ratios (Fig. S1). These land use change effects are amplified when accounting for unmeasured nighttime CO_2 increases in urban and cropland-dominated streams described above. Under these corrected CO_2 conditions, riverine N_2O emission is predicted to rise by 52 % (IQR= -12 – 170) for transitions from forest to cropland

catchments and by 161 % (IQR= 21 – 473) for shifts from forest to urban catchments. Based on these corrected values, we argue that as land use intensifies, mainly through agricultural expansion and urbanization from natural lands, these shifts in biogeochemical factors that regulate nitrification could substantially increase global riverine N_2O emissions.

4.4. Limitations of the study and targets for future research

While we were able to show that the positive CO_2 to N_2O relationship observed in global fluvial ecosystems may be related to enhanced nitrification in human-influenced rivers with low DOC:NO_3 ratios, our study was not without limitations. For example, the global dataset used to test some of the key hypotheses in this study includes sites sampled at different times and locations. Although the variance introduced by the nature of the data was accounted for in the mixed-effects models, questions remain as to whether the CO_2 fertilization effect on N_2O production is higher in certain regions or varies seasonally. The lack of process-based measurements on a global scale also means that the evidence from our global meta-analysis is primarily circumstantial, with factors such as similar sources for CO_2 and N_2O potentially playing an important role in explaining their positive relationship. Furthermore, it is still unclear based on our in vitro experiments how much of the N_2O produced originates directly from hydroxylamine oxidation or other nitrification-induced processes, such as incomplete denitrification and nitrifier denitrification (Jung et al., 2014; Stieglmeier et al., 2014; Wrage-Mönnig et al., 2018). The magnitude of the possible climate feedback also remains uncertain despite its potential global relevance. This is due to difficulties in predicting future riverine CO_2 and DOC:NO_3 trends, which may be impacted by drivers other than land use changes, such as climate change. Therefore, we suggest that future global studies need to be informed by advanced experiments such as using stable isotope approaches and microbial gene analysis to answer some of the questions above, primarily as the drivers and processes regulating N_2O production and consumption in rivers still remain uncertain relative to those of CO_2 and CH_4.

5. Conclusions

- The positive CO_2 effect on nitrification-driven net N_2O production from fluvial ecosystems demonstrated in this study may signify an important climate feedback mechanism.
- Future land use changes from natural ecosystems to cropland or urban areas may further enhance the effects of this climate feedback mechanism, thereby increasing the contribution of fluvial ecosystems to global GHG budgets.
- More research is needed to better understand how elevated instream CO_2 affects N_2O production processes in streams and the implications of these changes under global climate change.

Data and code availability

The compiled global and experimental data used in this study will be available upon request. This study's statistical analysis and figures were performed and produced with publicly available packages in R (version 4.3.2).

Funding

K.B.B received additional funding from the Pioneer Center for Landscape Research into Sustainable Futures (Land-CRAFT) (Land-CRAFT), DNRF Grant P2.

The TERENO Bavarian Alps/ Pre-Alps Observatory provided infrastructure funding for this study, which was funded by the Helmholtz Association through the joint Changing Earth—Sustaining our Future (PoF IV) program of Karlsruhe Institute of Technology (KIT).

CRediT authorship contribution statement

R.M. Mwanake: Writing – review & editing, Writing – original draft, Methodology, Formal analysis, Data curation, Conceptualization. **G.M. Gettel:** Writing – review & editing, Supervision, Conceptualization. **E.G. Wangari:** Writing – review & editing, Data curation. **G.W. Macharia:** Writing – review & editing, Data curation. **R. Martínez-Cuesta:** Writing – review & editing, Data curation. **S. Schulz:** Writing – review & editing, Resources, Methodology. **M. Schloter:** Writing – review & editing, Resources, Methodology. **K. Butterbach-Bahl:** Writing – review & editing, Supervision, Conceptualization. **R. Kiese:** Writing – review & editing, Supervision, Funding acquisition, Conceptualization.

Declaration of competing interest

The authors declare no competing interests.

Acknowledgements

We acknowledge all contributors to the GRiMeDB database, which provided part of the GHG concentration dataset for this study. We also thank the entire laboratory staff at KIT-IMK-IFU and Helmholtz Institute in Munich for providing support for chemical analysis.

Supplementary materials

Supplementary material associated with this article can be found, in the online version, at doi:10.1016/j.watres.2025.124320.

References

Aho, K.S., Maavara, T., Cawley, K.M., Raymond, P.A., 2023. Inland waters can act as nitrous oxide sinks: observation and modeling reveal that nitrous oxide undersaturation may partially offset emissions. Geophys. Res. Lett. 50 (21). https://doi.org/10.1029/2023GL104987.

Aho, K.S., Raymond, P.A., 2019. Differential response of greenhouse gas evasion to storms in forested and wetland streams. J. Geophys. Res.: Biogeosci. 124 (3), 649–662. https://doi.org/10.1029/2018JG004750.

Alexander, P., Rabin, S., Anthoni, P., Henry, R., Pugh, T.A.M., Rounsevell, M.D.A., Arneth, A., 2018. Adaptation of global land use and management intensity to changes in climate and atmospheric carbon dioxide. Glob. Change Biol. 24 (7), 2791–2809. https://doi.org/10.1111/gcb.14110.

Banerjee, S., Siciliano, S.D., 2012. Factors driving potential ammonia oxidation in Canadian arctic ecosystems: does spatial scale matter? Appl. Environ. Microbiol. 78 (2), 346–353. https://doi.org/10.1128/AEM.06132-11.

Baulch, H.M., Schiff, S.L., Maranger, R., Dillon, P.J., 2011. Nitrogen enrichment and the emission of nitrous oxide from streams. Glob. Biogeochem. Cycl. 25 (4). https://doi.org/10.1029/2011GB004047.

Beaulieu, J.J., Tank, J.L., Hamilton, S.K., Wollheim, W.M., Hall, R.O., Mulholland, P.J., Peterson, B.J., Ashkenas, L.R., Cooper, L.W., Dahm, C.N., Dodds, W.K., Grimm, N.B., Johnson, S.L., McDowell, W.H., Poole, G.C., Maurice Valett, H., Arango, C.P., Bernot, M.J., Burgin, A.J., Thomas, S.M., 2011. Nitrous oxide emission from denitrification in stream and river networks. Proc. Natl. Acad. Sci. U. S. A. 108 (1), 214–219. https://doi.org/10.1073/pnas.1011464108.

Bernhardt, E.S., Likens, G.E., 2002. Dissolved organic carbon enrichment alters nitrogen dynamics in a forest stream. Ecology 83 (6), 1689–1700. https://doi.org/10.1890/0012-9658(2002)083[1689:DOCEAN]2.0.CO;2.

Bolleter, W.T., Bushman, C.J., Tidwell, P.W., 1961. Spectrophotometric determination of ammonia as indophenol. Anal. Chem. 33, 592–594.

Borges, A.V., Darchambeau, F., Lambert, T., Morana, C., Allen, G.H., Tambwe, E., Toengaho Sembaito, A., Mambo, T., Nlandu Wabakhangazi, J., Descy, J.-P., Teodoru, C.R., Bouillon, S., 2019. Variations in dissolved greenhouse gases (CO_2, CH_4, N_2O) in the Congo River network overwhelmingly driven by fluvial-wetland connectivity. Biogeosciences 16 (19), 3801–3834. https://doi.org/10.5194/bg-16-3801-2019.

Casciotti, K.L., Ward, B.B., 2001. Dissimilatory nitrite reductase genes from autotrophic ammonia-oxidizing bacteria. Appl. Environ. Microbiol. 67 (5), 2213–2221. https://doi.org/10.1128/AEM.67.5.2213-2221.2001.

Casciotti, K.L., Ward, B.B., 2005. Phylogenetic analysis of nitric oxide reductase gene homologues from aerobic ammonia-oxidizing bacteria. FEMS Microbiol. Ecol. 52 (2), 197–205. https://doi.org/10.1016/j.femsec.2004.11.002.

Cébron, A., Garnier, J., Billen, G., 2005. Nitrous oxide production and nitrification kinetics by natural bacterial communitites of the lower Seine river (France). Aquat. Microb. Ecol. 41, 25–38. https://doi.org/10.3354/ame041025.

Chen, X., Wang, J., Liu, J., Zhang, S., Gao, H., Xia, X., 2025. Unveiling riverine N_2O dynamics along urbanization gradients by integrating hydrological, biogeochemical

and microbial processes. Water Res. 268, 122620. https://doi.org/10.1016/j.watres.2024.122620.
Chiriboga, G., Borges, A.V., 2023. Andean headwater and piedmont streams are hot spots of carbon dioxide and methane emissions in the Amazon basin. Commun. Earth Environ. 4 (1), 76. https://doi.org/10.1038/s43247-023-00745-1.
Cooper, T.G., Filmer, D., Wishnick, M., Lane, M.D., 1969. The active species of "CO_2" utilized by ribulose diphosphate carboxylase. J. Biol. Chem. 244 (4), 1081–1083. https://doi.org/10.1016/S0021-9258(18)91899-5.
Denecke, M., Liebig, T., 2003. Effect of carbon dioxide on nitrification rates. Bioprocess Biosyst. Eng. 25 (4), 249–253. https://doi.org/10.1007/s00449-002-0303-z.
Drake, T.W., Van Oost, K., Barthel, M., Bauters, M., Hoyt, A.M., Podgorski, D.C., Six, J., Boeckx, P., Trumbore, S.E., Cizungu Ntaboba, L., Spencer, R.G.M., 2019. Mobilization of aged and biolabile soil carbon by tropical deforestation. Nat. Geosci. 12 (7), 541–546. https://doi.org/10.1038/s41561-019-0384-9.
Duffner, C., Holzapfel, S., Wunderlich, A., Einsiedl, F., Schloter, M., Schulz, S., 2021. Dechloromonas and close relatives prevail during hydrogenotrophic denitrification in stimulated microcosms with oxic aquifer material. FEMS Microbiol. Ecol. 97 (3), fiab004. https://doi.org/10.1093/femsec/fiab004.
Gómez-Gener, L., Rocher-Ros, G., Battin, T., Cohen, M.J., Dalmagro, H.J., Dinsmore, K.J., Drake, T.W., Duvert, C., Enrich-Prast, A., Horgby, Å., Johnson, M.S., Kirk, L., Machado-Silva, F., Marzolf, N.S., McDowell, M.J., McDowell, W.H., Miettinen, H., Ojala, A.K., Peter, H., Sponseller, R.A., 2021. Global carbon dioxide efflux from rivers enhanced by high nocturnal emissions. Nat. Geosci. 14 (5), 289–294. https://doi.org/10.1038/s41561-021-00722-3.
Hama-Aziz, Z.Q., Hiscock, K.M., Cooper, R.J., 2017. Dissolved nitrous oxide (N_2O) dynamics in agricultural field drains and headwater streams in an intensive arable catchment. Hydrol. Process. 31 (6), 1371–1381. https://doi.org/10.1002/hyp.11111.
Harrison, J., Matson, P., 2003. Patterns and controls of nitrous oxide emissions from waters draining a subtropical agricultural valley. Glob. Biogeochem. Cycl. 17 (3). https://doi.org/10.1029/2002gb001991.
Helton, A.M., Ardón, M., Bernhardt, E.S., 2015. Thermodynamic constraints on the utility of ecological stoichiometry for explaining global biogeochemical patterns. Ecol. Lett. 18 (10), 1049–1056. https://doi.org/10.1111/ele.12487.
Herreid, A.M., Wymore, A.S., Varner, R.K., Potter, J.D., McDowell, W.H., 2021. Divergent controls on stream greenhouse gas concentrations across a land-use gradient. Ecosystems 24 (6), 1299–1316. https://doi.org/10.1007/s10021-020-00584-7.
Huesemann, M.H., Skillman, A.D., Crecelius, E.A., 2002. The inhibition of marine nitrification by ocean disposal of carbon dioxide. Mar. Pollut. Bull. 44 (2), 142–148. https://doi.org/10.1016/S0025-326X(01)00194-1.
Jiang, D., Khunjar, W.O., Wett, B., Murthy, S.N., Chandran, K., 2015. Characterizing the metabolic trade-off in Nitrosomonas europaea in response to changes in inorganic carbon supply. Environ. Sci. Technol. 49 (4), 2523–2531. https://doi.org/10.1021/es5043222.
Jung, M.Y., Well, R., Min, D., Giesemann, A., Park, S.J., Kim, J.G., Kim, S.J., Rhee, S.K., 2014. Isotopic signatures of N 2 O produced by ammonia-oxidizing archaea from soils. ISME J. 8 (5), 1115–1125. https://doi.org/10.1038/ismej.2013.205.
Kana, T.M., Darkangelo, C., Hunt, M.D., Oldham, J.B., Bennett, G.E., Cornwell, J.C., 1994. Membrane inlet mass spectrometer for rapid high-precision determination of N2, O2, and Ar in environmental water samples. Anal. Chem. 66 (23), 4166–4170. https://doi.org/10.1021/ac00095a009.
Kemp, M.J., Dodds, W.K., 2002. The influence of ammonium, nitrate, and dissolved oxygen concentrations on uptake, nitrification, and denitrification rates associated with prairie stream substrata. Limnol. Oceanogr. 47 (5), 1380–1393. https://doi.org/10.4319/lo.2002.47.5.1380.
Kottek, M., Grieser, J., Beck, C., Rudolf, B., Rubel, F., 2006. World map of the Köppen-Geiger climate classification updated. Meteorol. Z. 15 (3), 259–263. https://doi.org/10.1127/0941-2948/2006/0130.
Li, X., Zhou, Y., Eom, J., Yu, S., Asrar, G.R., 2019. Projecting global urban area growth through 2100 based on historical time series data and future shared socioeconomic pathways. Earth's Fut. 7 (4), 351–362. https://doi.org/10.1029/2019EF001152.
Lin, X., Lu, K., Hardison, A.K., Liu, Z., Xu, X., Gao, D., Gong, J., Gardner, W.S., 2021. Membrane inlet mass spectrometry method (REOX/MIMS) to measure 15N-nitrate in isotope-enrichment experiments. Ecol. Indic. 126. https://doi.org/10.1016/j.ecolind.2021.107639.
Madinger, H.L., Hall, R.O., 2019. Linking denitrification with ecosystem respiration in mountain streams. Limnol. Oceanogr. Lett. 4 (5), 145–154. https://doi.org/10.1002/lol2.10111.
Meyer, R.L., Allen, D.E., Schmidt, S., 2008. Nitrification and denitrification as sources of sediment nitrous oxide production: a microsensor approach. Mar. Chem. 110 (1), 68–76. https://doi.org/10.1016/j.marchem.2008.02.004.
Murphy, D.V., Recous, S., Stockdale, E.A., Fillery, I.R.P., Jensen, L.S., Hatch, D.J., Goulding, K.W.T., 2003. Gross nitrogen fluxes in soil : theory, measurement and application of 15N pool dilution techniques. In: Advances in Agronomy, 79. Academic Press, pp. 69–118. https://doi.org/10.1016/S0065-2113(02)79002-0.
Mwanake, R.M., Gettel, G.M., Aho, K.S., Namwaya, D.W., Masese, F.O., Butterbach-Bahl, K., Raymond, P.A., 2019. Land use, not stream order, controls N_2O concentration and flux in the upper mara river basin, Kenya. J. Geophys. Res.: Biogeosci. 124 (11), 3491–3506. https://doi.org/10.1029/2019JG005063.
Mwanake, R.M., Gettel, G.M., Ishimwe, C., Wangari, E.G., Butterbach-Bahl, K., Kiese, R., 2022. Basin-scale estimates of greenhouse gas emissions from the Mara River, Kenya: importance of discharge, stream size, and land use/land cover. Limnol. Oceanogr. 67 (8), 1776–1793. https://doi.org/10.1002/lno.12166.
Mwanake, R.M., Gettel, G.M., Wangari, E.G., Butterbach-Bahl, K., Kiese, R., 2023b. Interactive effects of catchment mean water residence time and agricultural area on water physico-chemical variables and GHG saturations in headwater streams. Front. Water 5. https://doi.org/10.3389/frwa.2023.1220544.
Mwanake, R.M., Gettel, G.M., Wangari, E.G., Glaser, C., Houska, T., Breuer, L., Butterbach-Bahl, K., Kiese, R., 2023a. Anthropogenic activities significantly increase annual greenhouse gas (GHG) fluxes from temperate headwater streams in Germany. Biogeosciences 20 (16), 3395–3422. https://doi.org/10.5194/bg-20-3395-2023.
Mwanake, R.M., Imhof, H.K., Kiese, R., 2024. Divergent drivers of the spatial variation in greenhouse gas concentrations and fluxes along the Rhine River and the Mittelland canal in Germany. Environ. Sci. Pollut. Res. https://doi.org/10.1007/s11356-024-33394-8.
Mwanake, R.M., Wangari, E.G., Winkler, K., Gretchen, G.M., Butterbach-Bahl, K., Kiese, R., 2025. From data to insights: upscaling riverine GHG fluxes in Germany with machine learning. Sci. Total Environ. 958, 177984. https://doi.org/10.1016/j.scitotenv.2024.177984.
Patton, C.J., Kryskalla, J.R., Survey, U.S.G., 2011. Colorimetric determination of nitrate plus nitrite in water by enzymatic reduction, automated discrete analyzer methods. Techniques and Methods. https://doi.org/10.3133/tm5B8.
Piatka, D.R., Nánási, R.L., Mwanake, R.M., Engelsberger, F., Willibald, G., Neidl, F., Kiese, R., 2024. Precipitation fuels dissolved greenhouse gas (CO_2, CH_4, N_2O) dynamics in a peatland-dominated headwater stream: results from a continuous monitoring setup. Front. Water 5. https://doi.org/10.3389/frwa.2023.1321137.
Quick, A.M., Reeder, W.J., Farrell, T.B., Tonina, D., Feris, K.P., Benner, S.G., 2019. Nitrous oxide from streams and rivers: a review of primary biogeochemical pathways and environmental variables. Earth-Sci. Rev. 191, 224–262. https://doi.org/10.1016/j.earscirev.2019.02.021.
Raymond, P.A., Caraco, N.F., Cole, J.J., 1997. Carbon dioxide concentration and atmospheric flux in the Hudson River. Estuaries 20 (2), 381–390. https://doi.org/10.2307/1352351.
Raymond, P.A., Hamilton, S.K., 2018. Anthropogenic influences on riverine fluxes of dissolved inorganic carbon to the oceans. Limnol. Oceanogr. Lett. 3 (3), 143–155. https://doi.org/10.1002/lol2.10069.
Regnier, P., Friedlingstein, P., Ciais, P., Mackenzie, F.T., Gruber, N., Janssens, I.A., Laruelle, G.G., Lauerwald, R., Luyssaert, S., Andersson, A.J., Arndt, S., Arnosti, C., Borges, A.V., Dale, A.W., Gallego-Sala, A., Goddéris, Y., Goossens, N., Hartmann, J., Heinze, C., Thullner, M., 2013. Anthropogenic perturbation of the carbon fluxes from land to ocean. Nat. Geosci. 6 (8), 597–607. https://doi.org/10.1038/ngeo1830.
Reichenpfader, T., Attermeyer, K., 2024. Stream <scp>CO $_2$ </scp>emissions are overestimated without consideration of diel water and atmospheric <scp>CO $_2$ </scp>variability. Limnol. Oceanogr. Lett. https://doi.org/10.1002/lol2.10405.
Reisinger, A.J., Tank, J.L., Hoellein, T.J., Hall, R.O., 2016. Sediment, water column, and open-channel denitrification in rivers measured using membrane-inlet mass spectrometry. J. Geophys. Res.: Biogeosci. 121 (5), 1258–1274. https://doi.org/10.1002/2015JG003261.
Robert Tabita, F., 1999. Microbial ribulose 1,5-bisphosphate carboxylase/oxygenase: a different perspective. In: Photosynthesis Research, 60.
Rosamond, M.S., Thuss, S.J., Schiff, S.L., 2012. Dependence of riverine nitrous oxide emissions on dissolved oxygen levels. Nat. Geosci. 5 (10), 715–718. https://doi.org/10.1038/ngeo1556.
Schumacker, R., Lomax, R., 2010. A Beginner's Guide to Structural Equation Modeling, 3rd Edition. Routledge. https://doi.org/10.4324/9780203851319.
Stanley, E.H., Loken, L.C., Casson, N.J., Oliver, S.K., Sponseller, R.A., Wallin, M.B., Zhang, L., Rocher-Ros, G., 2023. GRiMeDB: the global river methane database of concentrations and fluxes. Earth Syst. Sci. Data 15 (7), 2879–2926. https://doi.org/10.5194/essd-15-2879-2023.
Steuernagel, L., de Léon Gallegos, E.L., Azizan, A., Dampmann, A.K., Azari, M., Denecke, M., 2018. Availability of carbon sources on the ratio of nitrifying microbial biomass in an industrial activated sludge. Int. Biodeterior. Biodegrad. 129, 133–140. https://doi.org/10.1016/j.ibiod.2018.02.001.
Stieglmeier, M., Mooshammer, M., Kitzler, B., Wanek, W., Zechmeister-Boltenstern, S., Richter, A., Schleper, C., 2014. Aerobic nitrous oxide production through N-nitrosating hybrid formation in ammonia-oxidizing archaea. ISME J. 8 (5), 1135–1146. https://doi.org/10.1038/ismej.2013.220.
Strahler, A.N., 1952. Hypsometric (area-altitude) analysis of erosional topography. Gsa Bull. 63 (11), 1117–1142. https://doi.org/10.1130/0016-7606(1952)63[1117:haaoet]2.0.co;2.
Strauss, E.A., Lamberti, G.A., 2002. Effect of dissolved organic carbon quality on microbial decomposition and nitrification rates in stream sediments. Freshw. Biol. 47 (1), 65–74. https://doi.org/10.1046/j.1365-2427.2002.00776.x.
Strauss, E.A., Mitchell, N.L., Lamberti, G.A., 2002. Factors regulating nitrification in aquatic sediments: effects of organic carbon, nitrogen availability, and pH. Can. J. Fish. Aquat. Sci. 59 (3), 554–563. https://doi.org/10.1139/f02-032.
Taylor, P.G., Townsend, A.R., 2010. Stoichiometric control of organic carbon-nitrate relationships from soils to the sea. Nature 464 (7292), 1178–1181. https://doi.org/10.1038/nature08985.
Wachholz, A., Dehaspe, J., Ebeling, P., Kumar, R., Musolff, A., Saavedra, F., Winter, C., Yang, S., Graeber, D., 2023. Stoichiometry on the edge—humans induce strong imbalances of reactive C:N:P ratios in streams. Environ. Res. Lett. 18 (4). https://doi.org/10.1088/1748-9326/acc3b1.
Wang, C., Xv, Y., Wu, Z., Li, X., Li, S., 2024. Denitrification regulates spatiotemporal pattern of N_2O emission in an interconnected urban river-lake network. Water Res. 251, 121144. https://doi.org/10.1016/j.watres.2024.121144.
Wang, J., Wang, G., Zhang, S., Xin, Y., Jiang, C., Liu, S., He, X., McDowell, W.H., Xia, X., 2022. Indirect nitrous oxide emission factors of fluvial networks can be predicted by dissolved organic carbon and nitrate from local to global scales. Glob. Change Biol. 28 (24), 7270–7285. https://doi.org/10.1111/gcb.16458.

Wang, S., Lan, B., Yu, L., Xiao, M., Jiang, L., Qin, Y., Jin, Y., Zhou, Y., Armanbek, G., Ma, J., Wang, M., Jetten, M.S.M., Tian, H., Zhu, G., Zhu, Y.G., 2024. Ammonium-derived nitrous oxide is a global source in streams. Nat. Commun. 15 (1). https://doi.org/10.1038/s41467-024-48343-9.

Wangari, E.G., Mwanake, R.M., Kraus, D., Werner, C., Gettel, G.M., Kiese, R., Breuer, L., Butterbach-Bahl, K., Houska, T., 2022. Number of chamber measurement locations for accurate quantification of landscape-scale greenhouse gas fluxes: importance of land use, seasonality, and greenhouse gas type. J. Geophys. Res.: Biogeosci. 127 (9). https://doi.org/10.1029/2022JG006901.

Webster, J.R., Mulholland, P.J., Tank, J.L., Valett, H.M., Dodds, W.K., Peterson, B.J., Bowden, W.B., Dahm, C.N., Findlay, S., Gregory, S.V., Grimm, N.B., Hamilton, S.K., Johnson, S.L., Martí, E., Mcdowell, W.H., Meyer, J.L., Morrall, D.D., Thomas, S.A., Wollheim, W.M., 2003. Factors affecting ammonium uptake in streams – an inter-biome perspective. Freshw. Biol. 48 (8), 1329–1352. https://doi.org/10.1046/j.1365-2427.2003.01094.x.

Wei, J., Zhang, X., Xia, L., Yuan, W., Zhou, Z., Brüggmann, N., 2022. Role of chemical reactions in the nitrogenous trace gas emissions and nitrogen retention: a meta-analysis. Sci. Total Environ. 808, 152141. https://doi.org/10.1016/j.scitotenv.2021.152141.

Weiss, R.F., 1974. Carbon dioxide in water and seawater: the solubility of a non-ideal gas. Mar. Chem. 2 (3), 203–215. https://doi.org/10.1016/0304-4203(74)90015-2.

Weiss, R.F., Price, B.A., 1980. Nitrous oxide solubility in water and seawater. Mar. Chem. 8, 347–359. https://doi.org/10.1016/0304-4203(80)90024-9.

Winkler, K., Fuchs, R., Rounsevell, M., Herold, M., 2021. Global land use changes are four times greater than previously estimated. Nat. Commun. 12 (1). https://doi.org/10.1038/s41467-021-22702-2.

Winnick, M.J., 2021. Stream transport and substrate controls on nitrous oxide yields from hyporheic zone denitrification. AGU Adv. 2 (4). https://doi.org/10.1029/2021av000517.

Woodrow, R.L., White, S.A., Conrad, S.R., Wadnerkar, P.D., Rocher-Ros, G., Sanders, C. J., Holloway, C.J., Santos, I.R., 2024. Enhanced stream greenhouse gas emissions at night and during flood events. Limnol. Oceanogr. Lett. 9 (3), 276–285. https://doi.org/10.1002/lol2.10374.

Wrage-Mönnig, N., Horn, M.A., Well, R., Müller, C., Velthof, G., Oenema, O., 2018. The role of nitrifier denitrification in the production of nitrous oxide revisited. Soil Biol. Biochem. 123, A3–A16. https://doi.org/10.1016/j.soilbio.2018.03.020.

Xu, W., Wang, G., Liu, S., Wang, J., McDowell, W.H., Huang, K., Raymond, P.A., Yang, Z., Xia, X., 2024. Globally elevated greenhouse gas emissions from polluted urban rivers. Nat. Sustain. https://doi.org/10.1038/s41893-024-01358-y.

Yao, Y., Tian, H., Shi, H., Pan, S., Xu, R., Pan, N., Canadell, J.G., 2020. Increased global nitrous oxide emissions from streams and rivers in the Anthropocene. Nat. Clim. Change 10 (2), 138–142. https://doi.org/10.1038/s41558-019-0665-8.

Zhang, H., Lauerwald, R., Ciais, P., Van Oost, K., Guenet, B., Regnier, P., 2022. Global changes alter the amount and composition of land carbon deliveries to European rivers and seas. Commun. Earth Environ. 3 (1). https://doi.org/10.1038/s43247-022-00575-7.

Zhang, W., Li, H., Xiao, Q., Li, X., 2021. Urban rivers are hotspots of riverine greenhouse gas (N_2O, CH_4, CO_2) emissions in the mixed-landscape chaohu lake basin. Water Res. 189, 116624. https://doi.org/10.1016/j.watres.2020.116624.